Clonal relationships between Tph and Tfh cells in patients with SLE and in murine lupus

Takanori Sasaki[1,*], John Sowerby[1,*], Yinan Xiao[1], Runci Wang[1], Kathryne E. Marks[1], Alice Horisberger[1], Yidan Gao[1], Pui Y. Lee[3], Yujie Qu[2], Marc A. Sze[2], Stephen E. Alves[2], Marc C. Levesque[2], Keishi Fujio[4], Karen H. Costenbader[1], Deepak A. Rao[1]

[1]Division of Rheumatology, Inflammation, Immunity, Brigham and Women's Hospital and Harvard Medical School, Boston, MA, USA
[2]Merck & Co., Inc., Boston, MA, USA
[3]Division of Immunology, Boston Children's Hospital and Harvard Medical School, Boston, MA, USA
[4]Department of Allergy and Rheumatology, Graduate School of Medicine, The University of Tokyo, Tokyo, Japan

*equal contribution

Correspondence
Deepak Rao, MD PhD
Division of Rheumatology, Inflammation, Immunity
Brigham and Women's Hospital
Hale Building for Transformative Medicine, 6002R
60 Fenwood Road,
Boston, MA, USA
darao@bwh.harvard.edu

Keywords
Systemic lupus erythematosus
T follicular helper cell
T peripheral helper cell
T cell receptor repertoire

Abstract
Pathologic T cell-B cell interactions drive disease in systemic lupus erythematosus (SLE). The T cells that activate B cell responses include T peripheral helper (Tph) and T follicular helper (Tfh) cells, yet the developmental and clonal relationships between these B cell-helper T cell populations are unclear. Here we use T cell receptor (TCR) profiling to demonstrate clonal overlap between Tph and Tfh cells in the circulation of patients with SLE. Expanded Tph and Tfh cell clones persist over the course of 1 year in patients with a new diagnosis of SLE, and clones are observed to shift both from Tfh to Tph cells and from Tph to Tfh cells over time. High resolution analysis of cells sorted as Tph cells ($CXCR5^{-}$ $PD\text{-}1^{hi}$) and Tfh cells ($CXCR5^{+}$ $PD\text{-}1^{hi}$) from SLE patients revealed considerable heterogeneity among cells sorted as Tph cells and highlighted a specific cluster of cells that expressed transcriptomic features of activated B cell-helper T cells. This cell population, marked by expression of *TOX* and *CXCL13,* was found in both sorted Tph and Tfh cells, and was clonally linked in these two populations. Analysis of B cell-helper T cells in murine pristane-induced lupus demonstrated similar populations of Tph and Tfh cells in both lung and spleen with strong clonal overlap. T cell-specific loss of Bcl6 prevented accumulation of Tfh cells and reduced accumulation of Tph cells in pristane-treated mice, indicating a role for Bcl6 in the survival and expansion of both populations. Together, these observations demonstrate a shared developmental path among pathologically expanded Tph and Tfh cells in lupus. The persistence of expanded Tph and Tfh cells clones over time may impose barriers to induction of stable tolerance by immunosuppressive medications or by B cell depletion.

Introduction

Systemic lupus erythematosus (SLE) is a systemic autoimmune disease that can cause immune-mediated injury to multiple organs (*1*). Pathologic interactions of T cells and B cells and production of autoantibodies are core features of SLE immunopathology (*2*). Production of autoantibodies typically require both autoreactive B cells and help from autoreactive T cells, which express T cell receptors (TCR) capable of recognizing the targeted self-antigens. Analyses of circulating T cells from patients with SLE have demonstrated an increase in circulating CXCR5^{+} PD-1^{hi} T follicular helper (Tfh) cells, as well as a prominent increase in circulating CXCR5^{-} PD-1^{hi} T peripheral helper (Tph) cells (*3*–*7*). Both Tfh and Tph cells are considered "B cell-helper T cells," as they are capable of recruiting and activating B cells through production of the B cell chemoattractant CXCL13 and the cytokine IL-21, which is required to induce B cell differentiation into plasmablasts (PB) and age-associated B cells (ABC)(*3*, *8*, *9*). Expansion of circulating Tph and Tfh cells has been observed in multiple SLE patient cohorts, generally with higher frequencies in patients with active disease (*4*–*6*, *10*, *11*). Longitudinal studies have indicated that Tfh cell expansion in blood is clearest early in disease and may decrease over time, while Tph cell expansion persists into established disease (*12*). In a cohort of patients with lupus nephritis, the frequency of Tph cells, but not Tfh cells, correlated both with disease activity and the frequency of circulating ABCs (*4*). The developmental relationship between Tph and Tfh cells remains largely unknown.

One challenge in evaluating the relationships between these cell populations is that distinguishing B cell-helper T cells from other activated T cell populations phenotypically remains difficult. Tfh cells are defined in part by the expression of CXCR5, a chemokine receptor that follows the ligand CXCL13 to induce cell migration into follicles in secondary lymphoid organs, which contain high levels of CXCL13 produced either by T cells or stromal cells (*13*–*16*). More refined populations of active Tfh cells or germinal center Tfh cells can be identified by expression of high levels of expression of PD-1, ICOS, BCL6, and CXCR5 (*14*–*17*). Tfh cells require the transcription factor BCL6, such that absence of BCL6 prevents accumulation of Tfh cells in vivo (*18*–*20*). Identifying Tph cells, which can be functionally defined as B cell-helper T cells that lack CXCR5 and instead express migratory programs targeting non-lymphoid tissues, is more challenging. Tph cells are often quantified in patient samples as CXCR5^{-} PD-1^{hi} CD4 T cells (*3*–*6*); however, this gating strategy is likely to capture heterogenous populations that include other activated T cells. In patients with SLE and rheumatoid arthritis (RA), the CXCR5^{-} PD-1^{hi} T cell population is enriched for a B cell-helper transcriptomic signature, and these cells provide help to B cells in vitro, indicating a clear B cell-helper phenotype within this cell population in these diseases (*3*, *4*). However, the proportion of B cell-helper T cells versus other T cell effectors among circulating PD-1^{hi} T cells may vary across diseases. Single cell RNA-seq studies have illustrated transcriptomically separable populations of Tph and Tfh cells within inflamed tissue (*21*), both with B cell-helper transcriptional signatures, yet the ability to distinguish these cells transcriptomically in blood has not been established.

In addition to transcriptomic parallels, developmental links between T cell populations in human studies can be inferred from TCR profiling, which provides a tool to track T cell clones across space, time, and phenotype. Each individual T cell produced in the thymus expresses a unique TCR, which is passed on to all progeny from that individual T cell clone. The TCRs can thus be utilized as molecular "barcodes," enabling the tracking of each T cell's developmental trajectory. This clonal tracking approach can also be applied to longitudinal samples, making it possible to trace how specific T cell subsets evolve over time and into different subsets. This approach has been used to identify shared TCRs in target tissues and blood of patients with type I diabetes and expansion of antigen-specific TCRs during progression to disease (*22*, *23*), as well as the persistence of expanded T cell clones in circulation of patients with systemic sclerosis over time (*24*).

Here, we report detailed profiling of TCRs of specific T cell populations from the circulation of patients with SLE, including Tph cells, Tfh cells, T regulatory cells (Tregs), and comparator T cell populations, obtained at diagnosis, 6 months, and 1 year. We combine this with single-cell RNA/TCR profiling for additional cellular resolution to interrogate clonal relationships between Tph and Tfh cell populations in SLE patients. We further profile Tph and Tfh cells from lung and spleen of mice with pristane-induced lupus to track and manipulate the development of these cells in vivo. These studies demonstrate a strong TCR repertoire overlap between Tph and Tfh cells in both SLE patients and in murine pristane-induced lupus across different time points and different tissues, indicating a tight developmental link between Tph and Tfh cells.

Results

Persistent shared clones in bulk sorted Tph and Tfh cells from patients with SLE

To investigate how the TCR repertoires differ in each T cell subset and how they change over time in SLE, we performed TCR sequencing on T cell subsets sorted from PBMC of 9 patients with a new diagnosis of SLE. Samples were collected within 6 months of diagnosis, and then subsequently after 6 months and 12 months of follow up. TCR repertoire analysis was conducted on seven memory CD4 T cell populations ($CD25^+$ $CD127^-$ Tregs, $CXCR5^-$ $PD\text{-}1^{hi}$ [Tph], $CXCR5^+$ $PD\text{-}1^{hi}$ [Tfh], $CXCR5^-$ $PD\text{-}1^{int}$, $CXCR5^+$ $PD\text{-}1^{int}$, $CXCR5^-$ $PD\text{-}1^{low}$, and $CXCR5^+$ $PD\text{-}1^{low}$) (Figure 1A). Cells sorted as Tph cells ($CXCR5^-$ $PD\text{-}1^{hi}$) exhibited the highest degree of clonal expansion, with persistently high clonal expansion at each timepoint (Figure 1B, C). Comparison of the overlap of TCR repertoires across different subsets demonstrated substantial clonal overlap across T cell subsets within each patient (Supplementary Figure 1A). We observed significant TCR repertoire overlap between $CXCR5^-$ $PD\text{-}1^{hi}$ and $CXCR5^+$ $PD\text{-}1^{hi}$ cells (Figure 1D, indicated as '1'), as well as between $CXCR5^-$ $PD\text{-}1^{hi}$ and $CXCR5^-$ $PD\text{-}1^{int}$ cells (indicated as '2'), between $CXCR5^-$ $PD\text{-}1^{int}$ cells and $CXCR5^-$ $PD\text{-}1^{low}$ cells (indicated as '3'), and between $CXCR5^+$ $PD\text{-}1^{hi}$ and $CXCR5^+$ $PD\text{-}1^{int}$ cells (indicated as '4'). The significant repertoire overlap between $CXCR5^+$ $PD\text{-}1^{hi}$ and $CXCR5^-$ $PD\text{-}1^{hi}$ cells, which are well separated cytometrically, supports a developmental relationship between Tph and Tfh cells. TCRs of Tregs showed little clonal overlap with any other T cell subset. There was minimal TCR overlap across different patients, as expected (Supplementary Figure 1A). TCR profiling of T cell subsets from a cohort of 10 non-inflammatory control patients demonstrated a similar pattern of TCR repertoire overlap across cell subsets, suggesting that the clonal relationships between T cell populations are broadly applicable and not disease-specific (Supplementary Figure 1B).

Longitudinal analyses of T cell subsets from the SLE cohort indicated that $CXCR5^-$ $PD\text{-}1^{hi}$, $CXCR5^+$ $PD\text{-}1^{hi}$, and Treg populations have expanded TCR clones that persist over at least the first year after diagnosis (Figure 1E, F). The repertoire overlap between $CXCR5^-$ $PD\text{-}1^{hi}$ and $CXCR5^+$ $PD\text{-}1^{hi}$ cells was consistently observed when comparing samples from diagnosis versus 6 months later, and comparing diagnosis versus 1 year later (Figure 1E, F). In addition, unique TCR clones from $CXCR5^+$ $PD\text{-}1^{hi}$ cells, not shared with $CXCR5^-$ $PD\text{-}1^{hi}$ cells at baseline, were also detected in $CXCR5^-$ $PD\text{-}1^{hi}$ cells, and vice versa, at 6 months and 1 year (Supplementary Figure 1C), suggesting potential phenotype transitions within clones. Treg clones remained unique to the Treg subset without substantial appearance in $CXCR5^-$ $PD\text{-}1^{hi}$, $CXCR5^+$ $PD\text{-}1^{hi}$, or other T cell subset repertoires over time.

A cluster of transcriptomically active B cell-helper T cells within Tph and Tfh cell populations

To evaluate TCRs of cells sorted as Tph and Tfh cells at higher cellular resolution, we conducted scRNA/TCRseq on T cell subsets from 3 of the SLE patients in this cohort using PBMC collected at 18 months after enrollment. To unambiguously distinguish between $CXCR5^-$ $PD\text{-}1^{hi}$ (Tph) cells and $CXCR5^+$ $PD\text{-}1^{hi}$ (Tfh) cells, we sorted $CXCR5^-$ $PD\text{-}1^{hi}$, $CXCR5^+$ $PD\text{-}1^{hi}$, $CXCR5^-$ $PD\text{-}1^{int}$, $CXCR5^+$ $PD\text{-}1^{int}$, and $PD\text{-}1^{low}$ cells from non-Treg memory CD4 T cells, and then generated scRNA/TCRseq data on each sorted population. UMAP visualization of all cells identified nine clusters (Figure 2A-C), including clusters with features of C0 (Tfh), C1 (Th1), C2 (Th2), C3 (CTL), C4 (Th17), and C5 (TOX^+ $CXCL13^+$). Over 50% of $CXCR5^+$ $PD\text{-}1^{hi}$ cells clustered in C0. In addition, 13% of $CXCR5^+$ $PD\text{-}1^{hi}$ cells clustered in C5 and 12% clustered in C8 ($GZMK^+$). The C5 cluster expressed several genes associated with B cell-helper function, including *CXCL13*, *IL21*, *CD200*, and *ICOS*. In contrast to Tfh cells, $CXCR5^-$ $PD\text{-}1^{hi}$ cells were more heterogenous, with cells localized to several different clusters. 16% of these cells localized to cluster 5, such that only cells sorted as $PD\text{-}1^{hi}$ Tph or Tfh cells substantially contributed to the C5 cluster representing active B cell-helper T cells. To confirm the identity of C5 cells as activated B cell-helper T cells, we established a tissue Tph/Tfh signature score based on the top 100 genes distinctively expressed by Tph/Tfh clusters from rheumatoid arthritis synovial tissue, where Tph cells were initially described (*3*, *25*) (Cluster 1, 4 and 7 in Supplementary Figure 2). This Tph/Tfh signature score well highlighted the tissue Tph/Tfh clusters in kidney (*26*) and skin (*27*) in SLE (Supplementary Figure 1D). In addition, the Tph/Tfh signature score was highest in C5, indicating that this cluster expresses a prototype Tph/Tfh signature (Figure 2D). In addition, both $PD\text{-}1^{hi}$ populations contributed to a $GZMK^+$ cluster. In contrast, a separate cytotoxic T lymphocyte (CTL) cluster primarily contained cells from $CXCR5^-$ $PD\text{-}1^{hi}$ and $CXCR5^-$ $PD\text{-}1^{int}$ populations, without a contribution from $PD\text{-}1^{hi}$ $CXCR5^+$ cells. Across each of Th1, Th2 ,Th17, and TOX^{hi} $CXCL13^{hi}$ clusters, $CXCR5^-$ $PD\text{-}1^{hi}$ tended to have higher scores for the Tph gene signature as compared to $CXCR5^-$ $PD\text{-}1^{int}$ or $PD\text{-}1^{low}$ cells (Figure 2E).

TCR clonal overlap between circulating Tph and Tfh cell populations

We then assessed the TCR clonal relationships across the finer T cell clusters revealed by scRNA-seq. C3 containing CTL exhibited the most clonal expansion (Figure 3A, B). The presence of these highly clonally

expanded CTLs accounts for the high oligoclonality of CXCR5$^-$ PD-1^{hi} cells observed in Figure 1. Consistent with this, the extent of clonality of bulk CXCR5$^-$ PD-1^{hi} pool was strongly correlated with the frequency of Tbet$^+$ granzyme B$^+$ CXCR5$^-$ PD-1^{hi} CD4 T cells as quantified by mass cytometry analysis of the same samples (Supplementary Figure 1E). We then assessed the TCR clonality of CXCR5$^-$ PD-1^{hi} or CXCR5$^+$ PD-1^{hi} cells within each scRNA-seq cluster. C3 (CTL) from CXCR5$^-$ PD-1^{hi} cells exhibited the most oligoclonality, while large expanded clones could also be found in C5 (TOX$^+$ CXCL13$^+$), as well as C1 (Th1) and C8 (GZMK) (Figure 3C).

Analysis of the overall clonality of sorted populations using the scRNA-seq data recapitulated the same patterns of clonal overlap as observed in the bulk TCR analyses, including repertoire overlap between CXCR5$^-$ PD-1^{hi} and CXCR5$^+$ PD-1^{hi} cells and between PD-1$^{low/int/hi}$ CXCR5$^-$ populations (Supplementary Figure 1F). To determine the specific cell clusters that account for the clonal overlap between CXCR5$^-$ PD-1^{hi} and CXCR5$^+$ PD-1^{hi} cells observed in the bulk TCR data, we used the scTCR data to determine the proportion of TCRs in each single cell cluster that was detected in bulk TCR-seq data from the enrollment time point. TCRs from cluster C3 (CTL) were predominantly associated with the bulk CXCR5$^-$ PD-1^{hi} pool and were not found in the bulk CXCR5$^+$ PD-1^{hi} pool (Figure 3D). In contrast, TCRs from C5 (TOX$^+$ CXCL13$^+$) were found in both bulk CXCR5$^-$ PD-1^{hi} and CXCR5$^+$ PD-1^{hi} pools (Figure 3E). This pattern of shared Tph/Tfh clones in C5 but not in C3 was consistent across the 3 SLE patients (Figure 3D, E, Supplementary Figure 1G), indicating that cells with a B cell-helper signature, and not CTL, account for the clonal overlap in TCRs of bulk CXCR5$^-$ PD-1^{hi} and CXCR5$^+$ PD-1^{hi} pools. In addition, TCRs from C1 (Th1) and C3 (CTL) were shared between the CXCR5$^-$ PD-1^{hi} pool and the CXCR5$^-$ PD-1^{int} pool (Supplementary Figure 3A). In total, these results indicate shared B cell-helper T cell clones between PD-1^{hi} Tph and Tfh cells, which could be distinguished from large CTL clones found exclusively in the CXCR5$^-$ PD-1^{hi} pool and not in CXCR5$^+$ PD-1^{hi} Tfh cells.

To interrogate the direction of differentiation between C0 and C5, we next performed a pseudotime analysis. The pseudotime visualization indicated a trajectory from PD-1^{low} cells (C0) to CXCR5$^+$ PD-1^{int} (C0), Tfh (C0), Tfh (C5), and Tph (C5), with gradually increased expression of *TOX*, *CXCL13*, *IL21* and the tissue Tph/Tfh signature, but decreased expression of *CXCR5* and a naive T cell signature. Taken together, these TCR overlap results and pseudotime analysis suggest a potential transition from Tfh to Tph cell phenotypes.

TOX$^+$ IL21$^+$ CXCL13$^+$ T cells represent an activated proliferative B cell helper population in SLE
scRNA-seq analyses highlighted a population of T cells, captured in cluster C5, that expressed multiple B cell-helper features and was found specifically among CXCR5$^-$ PD-1^{hi} Tph and CXCR5$^-$ PD-1^{hi} Tfh cells. We surmised that the scRNA-seq analysis revealed a population of functionally active B cell-helper T cells in the circulation that is otherwise difficult to visualize; therefore, we sought to identify specific markers to more precisely capture the C5 population by cytometry. Analysis of differentially expressed genes (DEG) revealed *TOX*, *CD200*, *ICOS*, and proliferation markers such as *MKI67* and *CDK14* as preferentially expressed in C5 (Figure 4A), consistent with an activated, proliferative B cell-helper population. We then evaluated expression patterns of these markers in a mass cytometry dataset generated from the same patient cohort. ICOS$^+$ Ki67$^+$ cells were found to be most abundant in gated CXCR5$^-$ PD-1^{hi} cells and least abundant in PD-1^{low} cells, consistent with the scRNA-seq data (Supplement 3B, C, Figure 2A). Unsupervised clustering of cells in the mass cytometry dataset also identified a population of ICOS$^+$ Ki67$^+$ Tph/Tfh cells (Figure 4B, C). To test their association with SLE, we applied a Covarying Neighborhood Analysis (CNA) (*28*), which demonstrated that ICOS$^+$ Ki67$^+$ Tph/Tfh cells, Tregs, and granzyme K$^+$ CD4 T cells were significantly enriched in SLE patients compared to controls (Figure 4D). The proportion of ICOS$^+$ Ki67$^+$ Tph/Tfh cells was also significantly associated with the serum CXCL13 level, whereas that of total CXCR5$^+$ PD-1$^{hi/int}$ Tfh cells was not. ICOS$^+$ Ki67$^+$ Tph/Tfh cells were also significantly associated with the frequency of Ki67$^+$ plasmablasts quantified by mass cytometry and IGHV4-34, a well-known autoreactive BCR-IGHV chain (*29*, *30*), quantified by bulk BCR-seq (Figure 4E). Together, these results indicate that tracking an ICOS$^+$ Ki67$^+$ Tph/Tfh population captures an activated T cell population linked to overall T-B cell activation in SLE.

Next, to evaluate the C5 signature in additional cohorts of patients with SLE and other autoimmune diseases, we performed a deconvolution analysis using publicly available bulk RNA-seq data of CXCR3$^+$ Th1, CCR4$^+$ Th2, CCR6$^+$ Th17, and CXCR5$^+$ Tfh cells from 416 donors, including healthy controls and patients with 337 autoimmune diseases (*31*). Tph cells are not available in this dataset. C5 cells identified by deconvolution were observed in Th1, Th2, Th17, and CXCR5$^+$ Tfh populations, with a highest representation in the Tfh cell population. Compared to healthy controls, the proportion of C5 cells was

increased in SLE, mixed connective tissue disease, and idiopathic inflammatory myositis patient samples (Figure 4G). To further evaluate the association between the C5 population and plasmablasts, we examined the correlation using bulk RNA-seq data of plasmablasts from 57 SLE patients in this dataset (*31*). Consistent with our SLE cohort, we observed a significant correlation between the frequency of C5, as predicted by deconvolution, and MKI67 as well as IGHV4-34 among plasmablasts (Figure 4H).

CXCR5$^-$ PD-1^{hi} B cell-helper T cells accumulate in murine lupus

To evaluate whether the same heterogeneity and developmental links are observed among Tph cells in sites of inflammation, we evaluated PD-1^{hi} CD4 T cells in the murine model of pristane-induced lupus in C57BL/6 mice. By two weeks after pristane treatment, a population of cells expressing high levels of PD-1 but lacking CXCR5, resembling human Tph cells, accumulated in spleen and peritoneal fluid (Figure 5A). At time points after two months, these cells became detectable in the lungs, peritoneal fluid, and lipogranulomas within the peritoneal cavity. Notably, this population was also present in the spleen, along with Tfh cells.

To investigate the phenotype of these cells, we sorted T cell subsets from the spleen, draining lymph nodes, peritoneal granulomas, and lungs for RNA-seq (Figure 5B). Principal component analysis (PCA) revealed distinct clustering of cell types, with naïve cells, PD-1^{low} cells, and CXCR5$^-$ PD-1^{hi}/CXCR5$^+$ PD-1^{hi}/Treg cells forming separate clusters (Figure 5C). This clustering pattern was consistent across all tissues, although cells originating from the lungs clustered separately from other tissues. DEG analysis comparing CXCR5$^-$ PD-1^{hi} cells from spleen with naïve T cells revealed upregulation of genes associated with B cell help, including *Pdcd1*, *Icos*, and *Il21* in CXCR5$^-$ PD-1^{hi} cells (Figure 5C). Similar patterns were observed in other tissues (Supplementary Figure 4). Comparison of CXCR5$^-$ PD-1^{hi} with CXCR5$^+$ PD-1^{hi} cells revealed few DEGs, indicating a phenotypic similarity between the two populations. Consistent with human Tph cells, murine CXCR5$^-$ PD-1^{hi} cells exhibited lower expression of *Bcl6* and higher expression of *Prdm1* (Supplementary Figure 5). However, within the DEGs (splenic CXCR5$^-$ PD-1^{hi} vs naïve T cells), we also observed genes not typically associated with B cell-helper function, such as *Foxp3*, *Gzmk*, and *Eomes*, suggesting heterogeneity within the CXCR5$^-$ PD-1^{hi} population (Figure 5D). To explore how similar CXCR5$^-$ PD-1^{hi} cells were compared to other populations, we performed differential gene expression analysis against Treg and PD-1^{lo} populations in both the spleen and lung. We observed that there were fewer DEGs when CXCR5$^-$ PD-1^{hi} cells were used as the comparator population in contrast to CXCR5$^+$ PD-1^{hi} cells. These data suggested sorted CXCR5$^-$ PD-1^{hi} cells shared more transcriptional similarity to Tregs and PD-1^{lo} cells than do CXCR5$^+$ PD-1^{hi} cells (Figure 5E). By hierarchical clustering based on curated lists of genes relevant for these subsets, naïve cells, Tfh cells and PD-1^{low} cells from secondary lymphoid organs formed relatively homogeneous groups (Figure 5F). In contrast, CXCR5$^-$ PD-1^{hi} cells clustered with Tregs and PD-1^{low} cells from the lungs. While CXCR5$^-$ PD-1^{hi} cells clearly expressed genes important for B cell-helper function, they also expressed genes linked to Tregs, cytotoxicity, and other lineages, suggesting substantial heterogeneity.

Heterogeneity of B cell-helper T cells in spleen and lung

To better resolve the B cell-helper phenotype in CXCR5$^+$ PD-1^{hi} and CXCR5$^-$ PD-1^{hi} CD4 T cell populations in this model, we analyzed total CD4 T cells collected from spleen and lung of mice 12 months after pristane treatment by scRNA-seq. UMAP visualization of T cells from both spleen and lung identified 11 clusters (Figure 6A). One cluster in both spleen and lung (clusters 2 and 4) exhibited high expression of genes associated with B cell-helper function, including *Il21*, *Cxcr5*, *Pdcd1*, *Bcl6* and *Cd200* (Figure 6B). Expression of *Il21* was relatively selective to clusters 2 and 4 (Supplementary Figure 6). However, expression of these genes varied across the cluster, indicating further within-cluster heterogeneity (Figure 6C); therefore, we evaluated each cluster separately to unmask potential subcluster subset diversity. Cells within spleen cluster 2 segregated into four subpopulations (Figure 6D). Subcluster 2 showed a clear Tfh phenotype, with the highest expression of *Bcl6*, *Tox2*, and *Cxcr5* (Figure 6E). Analysis of lung cluster 4 showed a similar pattern, albeit with less distinction between Tph and transition Th inter subsets (Supplementary Figure 7A-B). Subcluster 1 had the highest expression of *Il21*, *Icos*, *Cd200*, *Tnfrs4* and transcription factor *Bhlhe40*, resembling some features shared with human Tph cells. Subcluster 0 showed an intermediate differentiation phenotype sharing some B cell helper molecule expression but also overlapping features with a Th1/GzmK state (subcluster 3). To evaluate the extent to which distinctions between subclusters 1 and 2 paralleled differences between bulk PD-1^{hi} CXCR5$^-$ and PD-1^{hi} CXCR5$^+$ cells, we evaluated expression of gene signatures defined from the bulk CXCR5$^-$ PD-1^{hi} and CXCR5$^+$ PD-1^{hi} pools in the single cell data. Genes overexpressed in CXCR5$^-$ PD-1^{hi} cells were highly enriched in subcluster 1 (Figure 6F, Supplementary Figure 7C). In contrast, genes overexpressed in the CXCR5$^+$ PD-1^{hi} pool showed higher expression in subcluster 2, which most resembled Tfh cells. Analysis of lung

subclusters showed a similar pattern to that observed in the spleen (Supplementary Figure 8D-E). Pseudo-bulk GSVA analysis further showed that spleen subcluster 1 enriched for a CXCR5^{-} PD-1^{hi} signature but not a CXCR5^{+} PD-1^{hi} signature, consistent with these cells being distinct from Tfh cells (Figure 6G). Lung Tph cells showed a broader enrichment of the CXCR5^{-} PD-1^{hi} gene signature which included the small number of Tfh cells detected in the lung (Supplementary Figure 7F). Finally, we used human-derived Tph and Tfh signatures to score B cell helper cluster in the spleen and lung. This showed enrichment of a human Tph signature in subcluster 1 of spleen and lung, consistent with these cells being transcriptionally similar with Tph cells (Supplementary Figure 7G).

DEG analysis directly comparing splenic subclusters 1 (Tph) and 2 (Tfh) showed upregulation of Tfh-associated genes *Cxcr5*, *Tox2*, *Bcl6*, *Pou2af1* and *Ascl2* in subcluster 2 (Figure 6H). In contrast, the subcluster 1 showed upregulation of genes important for calcium flux and IL-2 signalling (*Ahnak* and *Anxa6* respectively), as well as transcription factors *Id2* and *Bhlhe40*, both negative regulators of *Bcl6*. These cells also showed higher expression of OX40 (*Tnfrsf4*) and TNFR2 (*Tnfrsf1b*). GSEA analysis of a human Tph signature showed significant enrichment of genes upregulated in mouse Tph cells; in contrast murine Tfh cells showed significant enrichment of a tonsil derived Tfh signature (Figure 6I). Together, these results indicate that *Il21*-expressing T cell populations in the spleen and lung contain transcriptomically separable Tph and Tfh subsets.

Tph and Tfh cells in spleen and lung are clonally linked

We then used the scTCR-seq data of these cells to evaluate the clonal relationships between Tph, Tfh, and other cell states across tissues. Among all T cells, Gzmk^{+} clusters exhibited the highest degree of clonality in both the spleen and lung (Figure 7A). Quantification of TCR clonal sharing across clusters showed that B cell-helper clusters 2 and 4 in the spleen and lung showed the highest amount of sharing, indicating a developmental link between these two clusters (Figure 7B). To determine how transcriptionally defined Tph and Tfh cells from spleen and lung related to other clusters, we visualised and quantified how TCRs from each subcluster mapped across the broader phenotypic clusters (Figure 7C-E). Many of the splenic Tfh cells mapped to Gzmk^{+} clusters in the spleen, as well as lung B cell-helper clusters (Figure 7D). Splenic Tph cells showed more clonal sharing with lung B cell-helper clusters, consistent with migration of these cells from spleen to lung. Tfh cells in the lung had little overlap with any other cluster. In contrast, lung Tph cells showed clear links to splenic B cell-helper T cells and also to lung Gzmk^{+} cells (Figure 7E).

We next analysed the incidence of TCR sharing specifically between the B cell-helper populations in both the spleen and lung (Figure 7F). Splenic Tfh cells mostly shared TCRs with other splenic subclusters, consistent with Tfh cells showing limited migration to the lung. Quantification of TCR overlap, accounting for differences in abundance of TCRs, showed that splenic Tph and Tfh cell TCRs were highly overlapping (Figure 7G); splenic Tph TCRs were also highly overlapping with lung Tph cells, indicating migratory and/or developmental overlap. Th1 cells in the spleen and lung shared a distinct overlap pattern, suggesting a developmental trajectory separate from Tfh/Tph cells.

Absence of Bcl6 expression reduces accumulation of both Tph and Tfh cells

Given the shared transcriptomic features and clonal overlap between Tfh and Tph cells, we tested whether these cell populations share a common dependence on Bcl6, a transcription factor essential for Tfh cell differentiation and maintenance (*18–20*). We used a Bcl6-floxed CD4^{cre} model to delete Bcl6 from T cells in pristane-treated mice and analyzed T cells collected from lung and spleen 3 months after pristane treatment by scRNA-seq (Figure 8A). Assessment of cytokine expression showed selective expression of *Il21* in cluster 16 of spleen and part of cluster 10 in the lung (Supplementary Figure 10). Spleen cluster 16 was split into 5 subclusters with subcluster 1 (Spl SC1) (Figure 8B). Using a gene signature derived from differential gene expression analysis of Tfh vs Tph splenic subclusters in 12-month pristane treated mice, we observed enrichment for a Tfh signature within spleen SC1; a Tph signature was enriched in subclusters 0 (Spl SC0) and 2 (Spl SC2). Within the lung cluster 10 subclusters, subcluster 5 (Lung SC5) and subcluster 2 (Lung SC2) showed the highest enrichment for a Tfh and Tph signature, respectively (Figure 8C). TCR sharing patterns between Tfh and Tph cells in the spleen, and between lung and spleen *Il21*$^{+}$ regions, were similar to those in the prior analysis of 12-month pristane treated mice, as intersect analysis revealed extensive TCR sharing among splenic B cell helper clusters in lung and spleen (Figure 8D,E). Loss of Bcl6 expression caused a significant reduction in *Il21*+ clusters in both spleen and lung (Figure 8F). Subcluster analysis revealed loss of Tfh cells in both spleen and lung with deletion of Bcl6 (Figure 8G,H). Tph clusters in spleen (Spl SC0 and SC2), and in lung (Lung SC2) were also reduced but not completely absent. Consistent with reduction in these populations, loss of Bcl6 expression caused a significant decrease in anti-dsDNA IgG production, along with a non-significant decrease in total IgG

production (Figure 8I). Together these results show that Bcl6 promotes the generation of both Tph and Tfh cells, and that reduction of these cells is accompanied by reduced autoantibody production.

Discussion

Here we present a detailed analysis of Tph and Tfh cells from the circulation of patients with SLE and in induced murine lupus, in both cases demonstrating the shared transcriptomic and developmental features of these cell populations and their dynamics over time. Tph and Tfh cells from SLE patients show substantial overlap in their TCRs at multiple timepoints, consistent with analyses of similarly sorted T cells from lymph nodes of patients with HIV (*32*). Our scRNA-seq analyses of SLE T cell populations highlighted a specific cluster of PD-1^{hi} T cells with features activation and proliferation that showed the most clonal sharing among sorted Tph and Tfh cells, and trajectory analyses suggest that cells may transition from a Tfh phenotype to a terminal Tph phenotype. Expanded clones of both Tph and Tfh cells could be detected at multiple timepoints over 1 year, suggesting that pathologically expanded Tph and Tfh cell clones persist systemically in SLE patients. This persistence of clonally expanded Tph and Tfh cells may impose barriers to induction of stable tolerance by either traditional immunosuppressive agents or by B cell depletion.

Tph cells as originally described in RA synovial tissue expressed transcriptomic, cytometric, and functional features similar to Tfh cells, with a capacity to stimulate B cell differentiation in an IL-21-dependent manner (*3*). Cells with similar transcriptomic, cytometric, and functional features to RA synovial T cells can be found in the circulation as well (*33*), and many studies have reported quantification circulating Tph and Tfh cells in autoimmune disease patient cohorts (*34*), yet identifying Tph cells in the circulation has been hampered by the difficulty in discriminating Tph cells from other activated T cell populations (*34*). Here, the recognition via scRNA-seq of a specific cluster of T cells with transcriptional features of activation, present in both sorted Tph and Tfh cell populations and showing shared clonality, provides a valuable tool in identifying circulating B cell-helper T cells and distinguishing these cells from PD-1^{+} cytotoxic T cells. The C5 cluster exhibited the highest expression of a Tph/Tfh signature score derived from kidney Tph/Tfh cells, along with high expression of *TOX*, *MKI67*, *ICOS*, *CXCL13*, and *IL21,* which strongly resembles Tph cells in the RA joints (*3*). Cluster C5 cell abundance correlated with both IGHV4-34^{+} plasmablasts and Ki67^{+} plasmablasts in SLE patients, suggesting that that these T cells likely provide help to B cells. These findings align with previous observations that ICOS expression on PD-1^{hi} T cells enriches for B cell-helper function (*35*). C5 cluster cells also express TOX, a transcription factor that promotes exhaustion and PD-1 expression (*36*, *37*). Upregulation of TOX may suggest chronic antigen stimulation in these cells.

Parallel scRNA-seq analyses of CD4 T cells from murine pristane-induced lupus model demonstrated heterogenous populations of T cells that express features associated with B cell help, including Tfh cells as well as cells comparable to Tph cells, with strong TCR overlap between the populations in both spleen and lung. The varied B cell-helper T cell populations observed in this model are consistent prior reports indicating a range of phenotypes of B cell-helper T cells that differ from prototypical Bcl6^{hi} CXCR5^{hi} Tfh cells. This includes CXCR4^{+} extrafollicular helper T cells in murine lupus (*38*), as well as CXCR5^{-} Tfh-like cells in lungs of mice with chronic Ag-driven inflammation (*39*), and T resident helper cells observed in lungs of mice with influenza (*40*, *41*). Tox2, a factor related to Tox has been reported to alter the chromatin accessibility at the Bcl6 locus in Tfh cells (*42*).

The factors that control Tph cell differentiation are still being delineated (*43*). Compared to Tfh cells, Tph cells exhibit lower BCL6 expression (*3*), suggesting that BCL6 may not play a critical role in Tph cells. However, we find that absence of Bcl6 in T cells in pristane-treated mice substantially reduced Tph cell accumulation, particularly in spleen. Bcl6 is a repressive transcription factor that inhibits the expression of master regulators such as Tbx21, Gata3, and Rorc, which are responsible for the differentiation of Th1, Th2, and Th17 cells. Simultaneously, Bcl6 represses Id2, Runx2, Runx3, Klf2, and Prdm1, thereby promoting the expression of Tfh-related genes such as Cxcr5, Icos, Pdcd1, and Il21 (*44*, *45*). In humans, BCL6 is expressed at high levels in germinal center-Tfh (GC-Tfh) cells compared to PD-1^{low} cells or pre-Tfh cells (*46*). In studies that defined the central role of Bcl6 for Tfh cells, the impact of Bcl6 loss was quite specific to Tfh cells, with limited effects on non-Tfh cells noted (*18–20*). Given the clonal relationship between Tfh and Tph cells, it is possible that one major path to accumulation of Tph cells occurs through conversion of some Tfh cells into Tph cells, which would explain the loss of Tph cells in the absence of Bcl6. Consistent with this idea, in patients newly diagnosed with SLE, CXCR5^{-} PD-1^{hi} Tph cells are persistently expanded over at least 1 year, whereas CXCR5^{+} PD-1^{hi} Tfh cells decrease over time, suggesting a potential transition of Tfh cells into Tph cells during disease progression (*12*). Moreover, a previous study demonstrated that the TCR repertoire overlap was observed between Tph cells and Tfh cells, and Tph cells were depleted by a Bcl6 inhibitor along with Tfh cells in the NOD.Aire$^{GW/}$ neuropathy

murine model (*47*). Alternatively, it is possible that Tph cells can also differentiate independently of Tfh cells, yet in a Bcl6-dependent manner. Bcl6 expression occurs transiently in T cells during the early stages of activation (*48*); thus, it is possible that early Bcl6 activity is required to generate a Tph cell, perhaps in a shared Tfh/Tph-precursor T cell. Finally, given that some Tph cells still accumulated in the lungs of pristane-treated mice despite the absence of Bcl6, it is possible that some Tph cells develop independently of Bcl6 and are induced by other factors. Additional studies are required to understand the extent to which these paths contribute to Tph cell accumulation in different settings.

This study is limited by the relatively small cohort of SLE patients analyzed and the inability to study tissue samples from SLE patients. In addition, pristane-induced lupus is only 1 of multiple lupus models that can be studied. In both the human and murine studies, the incomplete sampling of TCRs, assessing a small portion of the total T cells in each individual, may under-represent the extent of clonal sharing across T cell populations and timepoints. Nonetheless, our study provides a new delineation of the clonal dynamics of Tph and Tfh cells in the circulation of SLE patients over time and across tissues in a murine model of lupus. The persistence of clonally expanded Tph and Tfh cells suggest that these expanded T cell clones may need to be targeted therapeutically to erase the autoimmune T cell response established early on in patients with SLE.

Competing interests

The work was performed in part with grant support from Merck & Co., Inc. D.A.R. reports grant support from Janssen and Bristol-Myers Squibb outside of the current report, and reports personal fees from AstraZeneca, Pfizer, Merck, Amgen, Scipher Medicine, GlaxoSmithKline, and Bristol-Myers Squibb. He is co-inventor on a patent using T peripheral helper cells as a biomarker of autoimmune diseases. Y.Q., M.A.S., S.E.A., and M.C.L. are employees of Merck & Co., Inc.

Acknowledgements

The work has been supported in part by funding from Merck & Co., Inc (to K.H.C. and D.A.R.), and by a Burroughs Wellcome Fund Career Award in Medical Sciences and National Institute of Arthritis and Musculoskeletal and Skin Diseases, NIH P01 AR070253 (to D.A.R.). The authors would like to thank the Center for Cellular Profiling at Brigham and Women's Hospital for cell sorting. We thank the Accelerating Medicines Partnership: RA/SLE Network for generation of the rheumatoid arthritis synovial scRNA-seq data. Data from the AMP RA/SLE Network were obtained from the ARK Portal (arkportal.synapse.org). We thank the ImmuNexUT (Immune Cell Gene Expression Atlas from the University of Tokyo) for sharing the bulk RNA-seq data for autoimmune diseases.

Author contributions

T.S. and J.S. conceived the project, performed experiments, analyzed data, and wrote the manuscript. Y.X. analyzed transcriptomic data. R.X., K.E.M., Y.G., and P.L. performed experiments. A.H. assisted with mass cytometry analysis. Y.Q., M.A.S., S.E.A., and M.C.L. participated in study design. K.F. generated transcriptomic data. K.H. and D.A.R. conceived the project, supervised the work, recruited the patients, and wrote the manuscript. All authors discussed the results and commented on the manuscript.

Methods

Patient samples

This study was approved by the research ethics committees, and informed consent was obtained from all participating patients for the collection of specimens. All SLE patients met the 1997 ACR classification criteria, the 2012 SLICC criteria, and the 2019 EULAR/ACR classification criteria (*49–51*). For the longitudinal SLE cohort used for TCR and BCR sequencing, 9 SLE patients were included who were within 6 months of disease diagnosis and had not received major immunosuppressive therapies (treatment with prednisone ≤10 mg and hydroxychloroquine was permitted), along with 10 non-inflammatory controls. Samples from the 9 SLE patients were collected at the time of enrollment, 6 months after enrollment, and 1 year after enrollment. For the correlation analysis between complement levels and GZMK+ CD4 T cells, 13 additional patients with established SLE were included. PBMC was isolated by density gradient centrifugation using Ficoll-Paque Plus (GE Healthcare) and cryopreserved in FBS with 10% DMSO via slow freezing, followed by storage in liquid nitrogen.

Bulk TCR and BCR sequencing

Frozen PBMC samples were thawed into RPMI Medium 1640 (Life Technologies #11875-085), supplemented with 10% heat-inactivated FBS (Life Technologies #16000044). The samples were stained

with flow cytometry antibodies for 30 minutes on ice. After staining, the cells were washed once in PBS with 1% BSA, passed through a 70 µm filter, and stained with 1ul of a 1:100 diluted Propidium Iodide Solution (BioLegend, #421301). 7 T cell subsets and 4 B cell subsets were directly sorted from the samples using a 5L BD FACSAria Fusion cell sorter into RLT lysis buffer kept on ice. The lysate was then frozen at -80°C until shipment to iRepertoire. Bulk TCRB sequencing data were generated from DNA, and bulk BCR-IGHV sequencing data from RNA. Each lysate was split into two samples to create duplicate data. Read count data for each sample were generated by iRepertoire, including CDR3 sequences, sequence read counts for each clone, and information on the identified V, D, and J genes. These data were subsequently loaded into R (v4.2.0) for further analysis. Non-productive sequences identified by IMGT/V-QUEST were removed, and the count data were analyzed using the Immunarch package.

Single-Cell RNA and TCR sequencing for human samples

Frozen PBMC samples from 3 out of 9 SLE patients were thawed in RPMI Medium 1640 with 10% FBS. Cells were incubated with an Fc receptor blocking solution, Human TruStain FcX™ (BioLegend), in Cell Staining Buffer (BioLegend) for 10 minutes at 4°C, followed by staining with flow antibodies for 30 minutes on ice. 5 T cell subsets, from non-Treg memory cells, were sorted into RPMI Medium 1640 with 10% FBS. After washing with Cell Staining Buffer, the cells were stained with a hashtag antibody (BioLegend) for 30 minutes on ice. Cells were then washed three times with Cell Staining Buffer, and 30,000 cells from each subset/donor were mixed. Then the cells were stained with TotalSeq™-C Human Universal Cocktail (BioLegend) for 30 minutes on ice, washed three times, and resuspended in 0.4% BSA in PBS. After counting live cells in 0.4% BSA in PBS using Trypan blue, a total of 160,000 cells in two batches were loaded onto a Chromium Next GEM Chip G (10x Genomics). cDNA and library preparation were conducted according to the manufacturer's protocol. mRNA libraries were sequenced using the Novaseq S4 flow cell (Illumina), and CITE-seq antibody-derived tag (ADT) libraries were sequenced using the HiSeq X Ten System (Illumina). Unique molecular identifier (UMI) counts for mRNA and ADT were quantified using Cell Ranger v7.1.1. FASTQ files were aligned to the GRCh38 human reference genome using Cell Ranger v7.1.1 (10x Genomics), and gene and ADT reads were quantified simultaneously using the Cell Ranger count.

The files were then processed with the Seurat R package (v5.1.0) (*52*). Expression of each hashing antibody was normalized using the centered-log ratio (CLR) method, followed by demultiplexing with the HTODemux function and a positive quantile of 0.99. Doublets and cells without hashtag staining were excluded. For quality control, we removed cells expressing fewer than 200 genes, more than 3,000 genes, or containing more than 10% of total UMIs associated with mitochondrial genes. After QC, mRNA expression was log-normalized (scale.factor = 10,000), and protein expression was normalized with CLR. The top 2,000 most highly variable genes, selected through variance stabilizing transformation, were scaled. Next, 20 principal components (PCs) were calculated based on mRNA data, and samples were batch-corrected using the Harmony R package. UMAP visualization and clustering (resolution = 0.5) were performed. Tissue Tph/Tfh signatures were calculated using the differentially expressed genes (DEGs) of cluster 4 in lupus kidney single-cell RNA-seq data with the AddModuleScore function in Seurat.

Sequencing reads for the TCR library were processed through the Cell Ranger workflow (v7.1.1). Reads were aligned to a TCR reference (vdj-GRCh38), productive contigs were filtered, and CDR3 sequences were identified for each cell. Cells with matching both CDR3alpha and CDR3beta were grouped into the same clonotype. Each cell's TCR was then paired with its transcriptomic data by matching cell barcodes. These files were then analyzed using the scRepertoire package (*53*).

Mass cytometry

Cryopreserved PBMC were thawed into RPMI Medium 1640 (Life Technologies #11875-085) supplemented with 5% heat-inactivated fetal bovine serum (Life Technologies #16000044), 1 mM GlutaMAX (Life Technologies #35050079), antibiotic-antimycotic (Life Technologies #15240062), 2 mM MEM non-essential amino acids (Life Technologies #11140050), 10 mM HEPES (Life Technologies #15630080), 2.5 x 10^{-5} M 2-mercaptoethanol (Sigma-Aldrich #M3148), 20 units/mL sodium heparin (Sigma-Aldrich #H3393), and 25 units/mL benzonase nuclease (Sigma-Aldrich #E1014). Cells were counted and 0.5-1x10^{6} cells from each sample were transferred to a polypropylene plate for staining. The samples were spun down and aspirated. 5 µM of cisplatin viability staining reagent (Fluidigm #201064) was added for two minutes and then diluted with culture media. After centrifugation, Human TruStain FcX Fc receptor blocking reagent (BioLegend #422302) was used at a 1:100 dilution in PBS with 2.5 g bovine serum albumin (Sigma Aldrich #A3059) and 100 mg of sodium azide (Sigma Aldrich #71289) for 10 minutes followed by incubation with conjugated surface antibodies for 30 minutes. All antibodies were obtained from the Harvard Medical Area CyTOF Antibody Resource and Core (Boston, MA). 16% stock paraformaldehyde (Fisher Scientific #O4042-500) dissolved in PBS was used at a final concentration of 4% formaldehyde for 10 minutes in order to fix the

samples before permeabilization with the FoxP3/Transcription Factor Staining Buffer Set (ThermoFisher Scientific #00-5523-00). The samples were incubated with SCN-EDTA coupled palladium based barcoding reagents for 15 minutes and then combined into a single sample. Conjugated intracellular antibodies were added into each tube and incubated for 30 minutes. Cells were then fixed with 1.6% formaldehyde for 10 minutes. DNA was labelled for 20 minutes with an 18.75 µM iridium intercalator solution (Fluidigm #201192B). Samples were subsequently washed and reconstituted in Milli-Q filtered distilled water in the presence of EQ Four Element Calibration beads (Fluidigm #201078) at a final concentration of $1x10^6$ cells/mL. Samples were acquired on a Helios CyTOF Mass Cytometer (Fluidigm). Cytometry data were normalized and debarcoded. Live cells were gated as DNA^+ $Live^+$ $Beads^-$ using FlowJo (BD). Batch-corrected total live cells, were then analyzed using the Seurat R package (v5.1.0) (*52*) for PCA, neighborhood analysis, and clustering visualized by UMAP. Cells associated with SLE were identified using CNA (*28*).

Mice and injection protocol

C57BL/6J, $Bcl6^{fl/fl}$, and CD4cre mice were purchased from Jackson Laboratory. To generate $Bcl6^{fl/fl}$ CD4cre heterozygotes, $Bcl6^{fl}$ mice were crossed to homozygosity before being were crossed with CD4Cre hemizygous mice. Cre +ve and -ve, sex-matched, littermate controls were used for experiments. Pristane-induced lupus was initiated by a one-time, 0.5ml injection of Pristane (Sigma). Mice were left for stated experimental time-frames and monitored weekly. Animal protocols used in this study were approved by Brigham and Women's Hospital Institutional Animal Care and Use Committee.

Mouse Cell sorting and sequencing

Mice were sacrificed and tissues were processed immediately for flow staining and sorting. In brief, spleen, lymphnode, granuloma and lung were harvested from mice and mechanically dissociated to form single cell suspensions. Lung tissue was further treated with 100 ug/ml liberase TL and 100 ug/ml DNase in RPMI (both Sigma) for 30 minutes at 37 degrees in a shaker. Digestion was quenched with excess media, cells were washed, strained and then incubated for a further 20 minutes at 37 degrees to allow re-upregulation of Cxcr5. All cells were filtered through a 70 micron filter prior to flow staining or hashing protocols.

Resuspended cells from the spleen and lung tissues were first incubated with Live/Dead Aqua (Thermo) and FcR block (Biolegend) in PBS for 10 mins at 4°C. Cells were then stained by standard protocols with hashing antibodies (Biolegend), cite-seq antibodies: ICOS, IA/IE, CD200, CXCR6, CCR2, and CX3CR1 (Biolegend), and a staining cocktail: CD45.2 PerCP-Cy5.5, B220 BV785, CD4 PE-Cy7, TCRb FITC, CD44 e450, CD62L A780, CD25 A700, IL7Ra BV650, PD1 APC and CXCR5 PE (Biolegend). For bulk-sequencing, 2000 cells were sorted based on the gating outlined in Figure 5 directly into TCL lysis buffer (Qiagen) with 1% bME (Sigma). Lysates were vortexed to ensure proper lysis and snap frozen on dry ice. Lysates were sequenced using SMART-Seq2 RNA-sequencing (Broad Institute). Raw fastq files were processed, mapped and reads quantified using Salmon. Further downstream analysis was carried out in R. For single cell sequencing, total CD4 T cells were sorted from either spleen or lung tissue into tubes containing 0.4% BSA-PBS. For both experiments equal numbers of cells from each mouse and/or genotype were sorted, counted, pooled and processed for 10X Chromium sequencing (Centre for Cellular Profiling BWH). Approximately 30K cells were used for the 12mo experiment (n = 5 mice), and 100K cells were used for the $Bcl6^{fl/fl}$ CD4cre-/+ experiment (n= 5 mice/group). Raw files were aligned with the reference mouse genome. Filtered reads were used for downstream analyses.

Mouse RNA-Seq Analysis

Salmon quantification files were read into R using the “tximeta” package and a metadata table generated based on mouse donor, organ, and cell type. Raw counts and the metadata table was used by DESeq2 to normalise and filter data. Extra filters based on expression levels across multiple samples, as well as removal of mitochondrial, olfactory, and genes of unknown function. Batch effects (between mice) were removed using “Limma”. PCA was performed using prcomp and plotted with ggtools2. Differential gene expression was carried out using DESeq2 and volcano plots generated using ggplot2 also. Vst transformed data was used to plot heatmaps and carry out hierarchical clustering (pheatmap function R).

Mouse scRNA-seq Analysis

Raw reads generated from Cell Ranger were loaded in R and analyzed by the Seurat R package. Low-quality cells with less than 200 genes or more than 10% mitochondrial content were removed from the dataset. HTO data was added to Seuratobject and then normalized. The HTODemux function clustered cells based on the normalized data and assigned labeled cells to their original samples. Each hashtag corresponded to one sample origin. Cells classified as either 'negative' or 'doublets' were removed from

downstream analysis. Filtered cohorts included: 20,794 cells and 16,793 cells from the spleen and lung tissues of wildtype mice treaded pristane for 12 months, respectively; 33,554 cells and 24,923 cells from the spleen and lung tissues of wildtype mice treaded pristane for 3 months, respectively; 33,791 cells and 23,051 cells from the spleen and lung tissues of Bcl6fl/fl CD4cre mice treaded pristane for 3 months, respectively. Raw reads of the rest cells were first normalized and scaled with the NormalizeData and ScaleData functions in Seurat, respectively. The top 2000 variable genes were detected by the mean variability plot of the "FindVariableFeatures" function, and then PCA dimensionality reduction was performed with default parameters. Harmony was performed to correct batch effects between mice or different cohorts. Dimension reduction analysis was performed based on the top 10 to 20 harmonized principal components with a low clustering resolution. Standard plotting tools in Seurat (DimPlot, FeaturePlot, DotPlot) were used to visualise gene and cluster expression. FindMarkers was used to carry differential gene expression and this was visualised using ggplot2. Enrichment analysis was carried out using the top 100 genes up in Tph vs Tfh cells in the spleen using the ReactomePA package. AddModuleScore (part of Seurat package) was used to look for enrichment of gene signatures within clusters. The top 50 genes up in Tfh (vs Tph) or Tph (vs Tfh) in the spleen were used to generate the signature.
TCR clonality analyses were performed with scRepertoire (v.1.7.2) R package. TCR sequences processed by Cell Ranger were exported and integrated with single-cell sequencing data by the combineExpression function. Cells with a single TCR α or β chain were removed from downstream analysis. Clonally expanded T cells were defined as T cells with both TCR-α and -β chains comprising identical VDJ genes and CDR3 nucleotides. The clonotype frequency was defined with default parameters: single (cell=1), small (1<cells ≤ 5), medium (5<cells ≤ 20), large (20<cells ≤ 100), and hyperexpanded (100<cells ≤ 500). The function DimPlot from the Seurat R package was used to visualize the distribution of clonotype frequency. To determine T cells from the same clone, TCR sequences of all the expanded cells in the certain cluster (clonotype frequency >1) were first extracted. The function highlightClonotypes in the scRepertoire R package was used to obtain the subset with the same TCR repertoire. Morisita plots were generated using standard functions in the scRepetoire package. The T cell clones were highlighted on the UMAP by DimPlot and ggplot2. Upset package in R was used to visualise TCR sharing intersections.

ELISA
Total IgG and dsDNA-IgG ELISA (Chondrex) were carried out on serum from Bcl6$^{fl/fl}$ CD4cre-/+ mice after 3 months of pristane treatment following the manufacturer's instructions.

Figure legends

Figure 1. Longitudinal changes of TCR/BCR repertoire features in SLE.

A. Schematic of TCR repertoire analysis in SLE. Bulk TCRs of Tph cells, Tfh cells, Tregs, and 4 other comparator CD4 T cell subsets were generated from blood of 9 patients with a new diagnosis of SLE, followed across 3 timepoints and 10 control donors. **B, C.** TCR clonality changes over time (SLE: n = 9). TCR clonality was assessed by calculating the mean of inversion Simpson Index (downsampled to 5000 reads) for the duplicates. P-values by Wilcoxon test. **D.** TCR repertoire overlap between Tph cells, Tfh cells, Tregs, and 4 other comparator CD4 T cell subsets in SLE (n = 9, downsampled to 5000 reads). **E.** TCR repertoire overlap between Tph cells, Tfh cells, and Tregs across baseline and 6 months (SLE: n = 9, downsampled to 5000 reads). **F.** TCR repertoire overlap between Tph cells, Tfh cells, and Tregs across baseline and 1 year (SLE: n = 7, downsampled to 5000 reads).

Figure 2. Single cell RNA-seq revealed activated B cell helper T cells.

A, B. Cluster composition of Tph, Tfh, CXCR5$^-$ PD-1^{int}, CXCR5$^+$ PD-1^{int}, and PD-1^{low} cells (SLE: n = 3). Tph, Tfh, CXCR5$^-$ PD-1^{int}, CXCR5$^+$ PD-1^{int}, and PD-1^{low} cells were sorted, and stained with Hashtag antibodies, and then generated the scRNA-seq data. **C.** Gene expression profiles of each cluster in Lupus PBMC scRNA-seq data. **D.** Tissue Tph/Tfh score of each cluster. **E.** Tissue Tph/Tfh score of Th1, Th2, Th17, and TOX$^+$ CXCL13$^+$ cells in PD-1^{low}, CXCR5$^-$ PD-1^{int}, and CXCR5$^-$ PD-1^{hi} populations.

Figure 3. Clonal and developmental link between Tfh and Tph cells.

A. Clonality of each cluster in Lupus PBMC scRNAseq data**. B.** Inversion Simpson Index of each cluster. **C.** Clonality of each cluster divided by sorted Tph and sorted Tfh cells. **D.** Frequencies of TCR repertoire of C3 from patient SYL3 detected in bulk TCR-seq data at enrollment. **E.** Frequencies of TCR repertoire of C5 from SYL3 detected in bulk TCR-seq data at enrollment. **F**. Pseudotime analysis between C0 and C5 divided in PD-1^{low}, CXCR5$^-$ PD-1^{int}, sorted Tfh and sorted Tph cells. **G**. Trend of gene expression, Tph/Tfh signature score, naive gene signature scores aligned along pseudotime.

Figure 4. C5 is a strong B cell activator population

A. Volcano plot for the DEGs between C5 and other clusters. Red: adj p values < 0.05, log2FC > 0.5, Green: adj p values > 0.05, Blue: adj p values < 0.05, log2FC < 0.5. **B.** UMAP CD4 T cell clustering of mass cytometry from 14 non-inflammatory controls and 9 SLE patient samples. **C.** Marker expression of each cluster in the UMAP. **D.** CNA of mass cytometry data corrected for age and sex. N =14 non-inflammatory controls, 9 SLE patients (baseline samples). Red indicates neighborhoods positively associated with SLE, and blue indicates negative association with SLE. **E.** Correlation between serum CXCL13 and the frequencies of ICOS$^+$ Ki67$^+$ Tph/Tfh cluster, Tfh cluster CXCR5$^+$ PD-1^{low} cluster, and naive cluster at the baseline SLE samples. **F.** Linear mixed effect model analysis between mass cytometry clusters and the frequencies of IGHV4-34 on PB quantified by BCR-seq and Ki67$^+$ PB quantified by mass cytometry. 27 SLE patient samples (9 SLE patients x 3 time points) were used, with time as fixed effect. **G.** Estimated proportion of C5 cells among total cells by deconvolution of ImmuNexUT bulk RNAseq from 416 donors (HC, healthy controls: 79, AAV, ANCA-associated vasculitis:22, AOSD, adult-onset Still's disease: 17, BD, Behcet's disease : 22, IIM, idiopathic myositis: 64, RA, rheumatoid arthritis:24, SSc, systemic sclerosis:64, TAK, Takayasu disease:16, MCTD, mixed connect tissue disease: 19, SjS, Sjogren syndrome:18, SLE, systemic lupus erytomatothus:57). **H.** Spearman's correlation between the estimated frequencies of C5 in ImmuNexUT study and expression of MKI67 and IGHV4-34 in plasmablasts. RNA-seq data from 57 SLE donors were used.

Figure 5. CXCR5$^-$ PD-1^{hi} CD4 T cells in mouse have a B cell helper signature

A. Quantification of CXCR5$^-$ PD-1^{hi} subset in pristane induced lupus in spleen (Spl), peritoneal fluid (PF), lung and granuloma (Grn) at indicated time-points. ANOVA results with indicated post-test significance. * p = <0.05, ** p = < 0.01, *** p = <0.001, n= 3-4 per experiment. Pool of 3 independent experiments. **B**. Sorting schematic of the RNA-seq experiment. **C**. PCA analysis of sorted cell subsets grouped by cell type (left) or tissue (right). **D**. DEG analysis of splenic CXCR5$^-$ PD-1^{hi} vs Tn subsets, or CXCR5$^-$ PD-1^{hi} vs CXCR5$^+$ PD-1^{hi} subsets. **E**. Frequency of DEGs for each pairwise comparison across both spleen and lung tissues. Genes up regulated in CXCR5$^-$ PD-1^{hi} or CXCR5$^-$ PD-1^{hi} cells vs comparator are marked as red and blue respectively. **F**. Heatmap of gene expression for a custom gene list comprised of lineage, functional, migratory and activation markers. Normalised gene expression is plotted (row normalised) and values are clustered on cell type (column).

Figure 6. scRNA-seq analysis of CD4 T cells in murine lupus show B cell cluster heterogeneity
A. UMAP plot showing clustering of cell populations for both spleen and lung tissues. **B**. Dot plot of relative gene expression for various functional T cell states. **C**. Feature plots of single gene expression for labelled genes. **D, E**. UMAP and dot plot of gene expression for spleen cluster 2 sub-clustering. **F**. UMAP projection showing module scoring of splenic cluster 2 subclusters using genes upregulated in $CXCR5^{-}$ $PD\text{-}1^{hi}$ cells (red) or $CXCR5^{+}$ $PD\text{-}1^{hi}$ (blue) derived bulk-sorted populations. **G**. UMAP plot of aggregate subcluster expression analysed by GSVA for signatures in (F). **H**. Differential gene expression between splenic Tph (subcluster 1) and Tfh (subcluster 2) subsets. Top 25 in each direction are annotated. **I**. GSEA analysis of DEGs in (H) using human derived Tph or Tfh signatures. Shown on the RHS are the genes contributing to the leading edge of the enrichment.

Figure 7. TCR analysis of B cell helper T cells
A. TCR expansion across the dataset in both spleen and lung. Single (1), Small (>1-5), Medium (>5-20), large (>20-100) and hyperexpanded (>100) are annotated on the plot. **B**. Upset plot of TCR sharing showing the occurrence of a TCR clone being shared between different clusters (number above bar). Only the top 15 comparisons are shown. Total TCRs for each cluster are shown on the right. **C**. TCR clones from spleen and lung Tph/Tfh subsets mapped onto the UMAP to show sharing across clusters. **D, E**. Quantification of C in both the spleen and lung, showing both the proportion of TCRs of either Tph/Tfh cells and the total number of shared TCRs. **F**. Upset plot as in B but for both the spleen and lung B cell helper subclusters. **G**. Morisita index plot of spleen and lung B cell helper subclusters.

Figure 8. Bcl6 is necessary for B cell helper T cell development
A. UMAP plot of CD4 T cells (both spleen and lung) from 3 month treated $Bcl6^{fl/fl}$ CD4Cre-/+ mice. **B, C.** Subclustering analysis of cluster 16 from spleen (**B**) or cluster 10 from lung (**C**) showing the DimPlot clusters (LHS) and module enrichment analysis for Tph (red) or Tfh (blue) signatures derived from DEG analysis of 12-month pristane treated mice comparing Tph and Tfh clusters in the spleen. **D**. DimPlot showing TCR sharing of Tfh subclusters from the spleen (Spleen SC1) or lung (Lung SC5), and Tph-like subclusters in spleen (Spleen SC0 and SC5) or lung (lung SC2) . **E.** Upset plot of TCR sharing incidence between the lung cluster 10 and spleen cluster 16 subclusters. **F**. Grouped bar graph showing cluster count stratified by genotype for *Il21*+ clusters 10 and 16. **G, H**. Grouped bar graph showing sub-cluster cell counts in either the spleen (**G**) or lung (**H**) stratified by genotype. **I**. ELISA of total IgG and dsDNA-IgG in wildtype or $Bcl6^{fl/fl}$ $CD4Cre^{+}$ mice. Mann-Whitney U test, ** $p = < 0.01$, n=4-6 per group.

Supplementary Figure 1. TCR repertoire features in SLE patients.
A. Heatmap of TCR repertoire overlap based on CDR3 beta similarity across all samples from longitudinal SLE patients (n = 378 samples). **B.** TCR repertoire overlap between Tph cells, Tfh cells, Tregs, and 4 other comparator CD4 T cell subsets in non-inflammatory controls (n = 10, downsampled to 5000 reads). **C.** Frequency of unique TCR repertoire to Tph or Tfh cells at baseline detected at 6 months or 1 year (Time B : n = 9, Time C : n = 7, downsampled to 5000 reads). **D.** Tissue Tph/Tfh score of lupus kidney scRNAseq clusters (*26*) and lupus skin scRNAseq clusters (*27*). **E.** Correlation analysis between Inversion Simpson Index (shown in Figure 1B) and frequencies of GZMB$^+$ Tbet$^+$ cells in CXCR5$^-$ PD-1^{hi} Tph cells using 9 baseline SLE samples. **F.** TCR repertoire overlap across flow-sorted populations: Tph, Tfh, CXCR5$^+$ PD-1^{int}, CXCR5$^-$ PD-1^{int}, and PD-1^{low} cells. **G.** The ratio of the proportion of CXCR5$^-$ PD-1^{hi} bulk TCR-seq reads matching scTCRseq in each cluster to the proportion of CXCR5$^+$ PD-1^{hi} bulk TCR-seq reads matching scTCRseq in each cluster (n = 3).

Supplementary Figure 2. Feature plots of B cell helper genes in CD4 T cells from human RA synovium.
Expression of several genes associated with Tph (cluster 4 and 7) and Tfh (cluster 1) cells in human CD4 T cells from RA synovium.

Supplementary Figure 3. TCR overlap and mass cytometric validation of C5 detected by scRNAseq.
A. Circos plot showing the TCR sequence overlap in each cluster between CXCR5$^-$ PD-1^{hi} cells and CXCR5$^-$ PD-1^{int} cells. **B**. ICOS$^+$ Ki67$^+$ cells in CXCR5$^-$ PD-1^{hi} Tph, CXCR5$^+$ PD-1^{hi} Tfh, CXCR5$^-$ PD-1^{int}, CXCR5$^+$ PD-1^{int}, CXCR5$^-$ PD-1^{low}, CXCR5$^+$ PD-1^{low} cells. **C.** Frequencies of **B** in 10 non-inflammatory controls and baseline 9 SLE samples**.** Mann-Whitney test was used for the comparison.

Supplementary Figure 4. Differential gene expression analysis between CXCR5- PD-1^{hi} and naïve T cells across different tissues.
A. Volcano plot of differentially expressed genes between lung naïve CD4 T cells and lung CXCR5- PD-1^{hi} CD4 T cells. Several significant DEGs are annotated relating to naïve, Th1, Treg and B cell helper function. **B.** Volcano plot of differentially expressed genes between lymph node naïve CD4 T cells and lymph node CXCR5- PD-1^{hi} CD4 T cells. Several significant DEGs are annotated relating to naïve, Th1, Treg and B cell helper function. **C.** Volcano plot of differentially expressed genes between granuloma naïve CD4 T cells and granuloma CXCR5- PD-1^{hi} CD4 T cells. Several significant DEGs are annotated relating to naïve, Th1, Treg and B cell helper function.

Supplementary Figure 5. Gene expression bar plots of different sorted subsets in individual tissues.
A. Expression of *Prdm1* grouped by tissue for each sorted cell subset. Normalised counts are used, -/+ SD for 3-5 mice. **B**. Expression of *Bcl6* grouped by tissue for each sorted cell subset. Normalised counts are used, -/+ SD for 3-5 mice.

Supplementary Figure 6. Cytokine expression across CD4 T cell clusters in spleen and lung
Feature Plots of cytokine expression across the spleen and lung clusters.

Supplementary Figure 7. Subcluster analysis reveals distinct transcriptional states within spleen and lung
A. DimPlot showing subcluster analysis of lung cluster 4. **B.** DotPlot of gene expression for various functional T cell states. **C**. Single cell GSVA scoring of spleen subclusters with ANOVA analysis and Tukey's post-hoc testing. *** $p = <0.001$ **D**. UMAP projection showing module scoring of lung cluster 4 subclusters using genes upregulated in CXCR5- PD1^{hi} cells (red) or CXCR5+ PD1^{hi} (blue) derived bulk-sorted populations. **E**. Single cell GSVA scoring of lung subclusters with ANOVA analysis and Tukey's post-hoc testing.* $p = < 0.05$, ** $p = < 0.01$, *** $p = <0.001$. **F**. UMAP plot of aggregate lung subcluster expression analysed by GSVA for signatures in (Figure 6F). **G**. Module scoring of spleen and lung subclusters using human derived Tph and Tfh signatures.

Supplementary Figure 8 Cytokine expression across CD4 T cells clusters in CD4 T cells from Bcl6 sufficient or deficient mice
A. FeaturePlot expression of *Il21*, *Il10* and *Il2*. **B**. DotPlot of several different cytokines representative of different T cell functional states.

References

1. G. C. Tsokos, Systemic lupus erythematosus. *N. Engl. J. Med.* **365**, 2110–2121 (2011).

2. S. A. Jenks, K. S. Cashman, M. C. Woodruff, F. E.-H. Lee, I. Sanz, Extrafollicular responses in humans and SLE. *Immunol. Rev.* **288**, 136–148 (2019).

3. D. A. Rao, M. F. Gurish, J. L. Marshall, K. Slowikowski, C. Y. Fonseka, Y. Liu, L. T. Donlin, L. A. Henderson, K. Wei, F. Mizoguchi, N. C. Teslovich, M. E. Weinblatt, E. M. Massarotti, J. S. Coblyn, S. M. Helfgott, Y. C. Lee, D. J. Todd, V. P. Bykerk, S. M. Goodman, A. B. Pernis, L. B. Ivashkiv, E. W. Karlson, P. A. Nigrovic, A. Filer, C. D. Buckley, J. A. Lederer, S. Raychaudhuri, M. B. Brenner, Pathologically expanded peripheral T helper cell subset drives B cells in rheumatoid arthritis. *Nature* **542**, 110–114 (2017).

4. A. V. Bocharnikov, J. Keegan, V. S. Wacleche, Y. Cao, C. Y. Fonseka, G. Wang, E. S. Muise, K. X. Zhang, A. Arazi, G. Keras, Z. J. Li, Y. Qu, M. F. Gurish, M. Petri, J. P. Buyon, C. Putterman, D. Wofsy, J. A. James, J. M. Guthridge, B. Diamond, J. H. Anolik, M. F. Mackey, S. E. Alves, P. A. Nigrovic, K. H. Costenbader, M. B. Brenner, J. A. Lederer, D. A. Rao, Accelerating Medicines Partnership (AMP) RA/SLE Network, PD-1hiCXCR5- T peripheral helper cells promote B cell responses in lupus via MAF and IL-21. *JCI Insight* **4** (2019).

5. A. Makiyama, A. Chiba, D. Noto, G. Murayama, K. Yamaji, N. Tamura, S. Miyake, Expanded circulating peripheral helper T cells in systemic lupus erythematosus: association with disease activity and B cell differentiation. *Rheumatology (Oxford)* **58**, 1861–1869 (2019).

6. J. Lin, Y. Yu, J. Ma, C. Ren, W. Chen, PD-1+CXCR5-CD4+T cells are correlated with the severity of systemic lupus erythematosus. *Rheumatology (Oxford)* **58**, 2188–2192 (2019).

7. A. Horisberger, A. Griffith, J. Keegan, A. Arazi, J. Pulford, E. Murzin, K. Howard, B. Hancock, A. Fava, T. Sasaki, T. Ghosh, J. Inamo, R. Beuschel, Y. Cao, K. Preisinger, M. Gutierrez-Arcelus, T. M. Eisenhaure, J. Guthridge, P. J. Hoover, M. Dall'Era, D. Wofsy, D. L. Kamen, K. C. Kalunian, R. Furie, M. Belmont, P. Izmirly, R. Clancy, D. Hildeman, E. S. Woodle, W. Apruzzese, M. A. McMahon, J. Grossman, J. L. Barnas, F. Payan-Schober, M. Ishimori, M. Weisman, M. Kretzler, C. C. Berthier, J. B. Hodgin, D. S. Demeke, C. Putterman, Accelerating Medicines Partnership: RA/SLE Network, M. B. Brenner, J. H. Anolik, S. Raychaudhuri, N. Hacohen, J. A. James, A. Davidson, M. A. Petri, J. P. Buyon, B. Diamond, F. Zhang, J. A. Lederer, D. A. Rao, Blood immunophenotyping identifies distinct kidney histopathology and outcomes in patients with lupus nephritis. *bioRxivorg*, doi: 10.1101/2024.01.14.575609 (2024).

8. S. A. Jenks, K. S. Cashman, E. Zumaquero, U. M. Marigorta, A. V. Patel, X. Wang, D. Tomar, M. C. Woodruff, Z. Simon, R. Bugrovsky, E. L. Blalock, C. D. Scharer, C. M. Tipton, C. Wei, S. S. Lim, M. Petri, T. B. Niewold, J. H. Anolik, G. Gibson, F. E.-H. Lee, J. M. Boss, F. E. Lund, I. Sanz, Distinct Effector B Cells Induced by Unregulated Toll-like Receptor 7 Contribute to Pathogenic Responses in Systemic Lupus Erythematosus. *Immunity* **49**, 725-739.e6 (2018).

9. D. A. Rao, T cells that help B cells in chronically inflamed tissues. *Front. Immunol.* **9**, 1924 (2018).

10. J. He, L. M. Tsai, Y. A. Leong, X. Hu, C. S. Ma, N. Chevalier, X. Sun, K. Vandenberg, S. Rockman, Y. Ding, L. Zhu, W. Wei, C. Wang, A. Karnowski, G. T. Belz, J. R. Ghali, M. C. Cook, D. S. Riminton, A. Veillette, P. L. Schwartzberg, F. Mackay, R. Brink, S. G. Tangye, C. G. Vinuesa, C. R. Mackay, Z. Li, D. Yu, Circulating precursor CCR7(lo)PD-1(hi) CXCR5^{+} CD4^{+} T cells indicate Tfh cell activity and promote antibody responses upon antigen reexposure. *Immunity* **39**, 770–781 (2013).

11. J.-Y. Choi, J. H.-E. Ho, S. G. Pasoto, V. Bunin, S. T. Kim, S. Carrasco, E. F. Borba, C. R. Gonçalves, P. R. Costa, E. G. Kallas, E. Bonfa, J. Craft, Circulating follicular helper-like T cells in systemic lupus erythematosus: association with disease activity: Circulating tfh-like cells in SLE. *Arthritis Rheumatol.* **67**, 988–999 (2015).

12. T. Sasaki, S. Bracero, J. Keegan, L. Chen, Y. Cao, E. Stevens, Y. Qu, G. Wang, J. Nguyen, J. A. Sparks, V. M. Holers, S. E. Alves, J. A. Lederer, K. H. Costenbader, D. A. Rao, Longitudinal immune cell profiling in patients with early systemic lupus erythematosus. *Arthritis Rheumatol.* **74**, 1808–1821 (2022).

13. H. Yoshitomi, S. Kobayashi, A. Miyagawa-Hayashino, A. Okahata, K. Doi, K. Nishitani, K. Murata, H. Ito, T. Tsuruyama, H. Haga, S. Matsuda, J. Toguchida, Human Sox4 facilitates the development of CXCL13-producing helper T cells in inflammatory environments. *Nat. Commun.* **9**, 3762 (2018).

14. S. Crotty, T follicular helper cell biology: A decade of discovery and diseases. *Immunity* **50**, 1132–1148 (2019).

15. W. Song, J. Craft, T follicular helper cell heterogeneity: Time, space, and function. *Immunol. Rev.* **288**, 85–96 (2019).

16. H. Yoshitomi, H. Ueno, Shared and distinct roles of T peripheral helper and T follicular helper cells in human diseases. *Cell. Mol. Immunol.* **18**, 523–527 (2021).

17. X. Liu, R. I. Nurieva, C. Dong, Transcriptional regulation of follicular T-helper (Tfh) cells. *Immunol. Rev.* **252**, 139–145 (2013).

18. R. I. Nurieva, Y. Chung, G. J. Martinez, X. O. Yang, S. Tanaka, T. D. Matskevitch, Y.-H. Wang, C. Dong, Bcl6 mediates the development of T follicular helper cells. *Science* **325**, 1001–1005 (2009).

19. R. J. Johnston, A. C. Poholek, D. DiToro, I. Yusuf, D. Eto, B. Barnett, A. L. Dent, J. Craft, S. Crotty, Bcl6 and Blimp-1 are reciprocal and antagonistic regulators of T follicular helper cell differentiation. *Science* **325**, 1006–1010 (2009).

20. D. Yu, S. Rao, L. M. Tsai, S. K. Lee, Y. He, E. L. Sutcliffe, M. Srivastava, M. Linterman, L. Zheng, N. Simpson, J. I. Ellyard, I. A. Parish, C. S. Ma, Q.-J. Li, C. R. Parish, C. R. Mackay, C. G. Vinuesa, The transcriptional repressor Bcl-6 directs T follicular helper cell lineage commitment. *Immunity* **31**, 457–468 (2009).

21. F. Zhang, A. H. Jonsson, A. Nathan, N. Millard, M. Curtis, Q. Xiao, M. Gutierrez-Arcelus, W. Apruzzese, G. F. M. Watts, D. Weisenfeld, S. Nayar, J. Rangel-Moreno, N. Meednu, K. E. Marks, I. Mantel, J. B. Kang, L. Rumker, J. Mears, K. Slowikowski, K. Weinand, D. E. Orange, L. Geraldino-Pardilla, K. D. Deane, D. Tabechian, A. Ceponis, G. S. Firestein, M. Maybury, I. Sahbudin, A. Ben-Artzi, A. M. Mandelin 2nd, A. Nerviani, M. J. Lewis, F. Rivellese, C. Pitzalis, L. B. Hughes, D. Horowitz, E. DiCarlo, E. M. Gravallese, B. F. Boyce, Accelerating Medicines Partnership: RA/SLE Network, L. W. Moreland, S. M. Goodman, H. Perlman, V. M. Holers, K. P. Liao, A. Filer, V. P. Bykerk, K. Wei, D. A. Rao, L. T. Donlin, J. H. Anolik, M. B. Brenner, S. Raychaudhuri, Deconstruction of rheumatoid arthritis synovium defines inflammatory subtypes. *Nature* **623**, 616–624 (2023).

22. A. M. Mitchell, E. E. Baschal, K. A. McDaniel, K. M. Simmons, L. Pyle, K. Waugh, A. K. Steck, L. Yu, P. A. Gottlieb, M. J. Rewers, M. Nakayama, A. W. Michels, Temporal development of T cell receptor repertoires during childhood in health and disease. *JCI Insight* **7** (2022).

23. A. M. Mitchell, E. E. Baschal, K. A. McDaniel, T. Fleury, H. Choi, L. Pyle, L. Yu, M. J. Rewers, M. Nakayama, A. W. Michels, Tracking DNA-based antigen-specific T cell receptors during progression to type 1 diabetes. *Sci. Adv.* **9**, eadj6975 (2023).

24. N. H. Servaas, F. Zaaraoui-Boutahar, C. G. K. Wichers, A. Ottria, E. Chouri, A. J. Affandi, S. Silva-Cardoso, M. van der Kroef, T. Carvalheiro, F. van Wijk, T. R. D. J. Radstake, A. C. Andeweg, A. Pandit, Longitudinal analysis of T-cell receptor repertoires reveals persistence of antigen-driven CD4+ and CD8+ T-cell clusters in systemic sclerosis. *J. Autoimmun.* **117**, 102574 (2021).

25. F. Zhang, K. Wei, K. Slowikowski, C. Y. Fonseka, D. A. Rao, S. Kelly, S. M. Goodman, D. Tabechian, L. B. Hughes, K. Salomon-Escoto, G. F. M. Watts, A. H. Jonsson, J. Rangel-Moreno, N. Meednu, C. Rozo, W. Apruzzese, T. M. Eisenhaure, D. J. Lieb, D. L. Boyle, A. M. Mandelin 2nd, Accelerating Medicines Partnership Rheumatoid Arthritis and Systemic Lupus Erythematosus (AMP RA/SLE) Consortium, B. F. Boyce, E. DiCarlo, E. M. Gravallese, P. K. Gregersen, L. Moreland, G. S. Firestein, N. Hacohen, C. Nusbaum, J. A. Lederer, H. Perlman, C. Pitzalis, A. Filer, V. M. Holers, V. P. Bykerk, L. T. Donlin, J. H. Anolik, M. B. Brenner, S. Raychaudhuri, Defining inflammatory cell states in rheumatoid arthritis joint synovial tissues by integrating single-cell transcriptomics and mass cytometry. *Nat. Immunol.* **20**, 928–942 (2019).

26. A. Arazi, D. A. Rao, C. C. Berthier, A. Davidson, Y. Liu, P. J. Hoover, A. Chicoine, T. M. Eisenhaure, A. H. Jonsson, S. Li, D. J. Lieb, F. Zhang, K. Slowikowski, E. P. Browne, A. Noma, D. Sutherby, S. Steelman, D. E. Smilek, P. Tosta, W. Apruzzese, E. Massarotti, M. Dall'Era, M. Park, D. L. Kamen, R. A. Furie, F. Payan-Schober, W. F. Pendergraft 3rd, E. A. McInnis, J. P. Buyon, M. A. Petri, C. Putterman, K. C. Kalunian, E. S. Woodle, J. A. Lederer, D. A. Hildeman, C. Nusbaum, S. Raychaudhuri, M. Kretzler, J. H. Anolik, M. B. Brenner, D. Wofsy, N. Hacohen, B. Diamond, Accelerating Medicines Partnership in SLE network, The immune cell landscape in kidneys of patients with lupus nephritis. *Nat. Immunol.* **20**, 902–914 (2019).

27. G. S. Dunlap, A. C. Billi, X. Xing, F. Ma, M. P. Maz, L. C. Tsoi, R. Wasikowski, J. B. Hodgin, J. E. Gudjonsson, J. M. Kahlenberg, D. A. Rao, Single-cell transcriptomics reveals distinct effector profiles of infiltrating T cells in lupus skin and kidney. *JCI Insight* **7** (2022).

28. Y. A. Reshef, L. Rumker, J. B. Kang, A. Nathan, I. Korsunsky, S. Asgari, M. B. Murray, D. B. Moody, S. Raychaudhuri, Co-varying neighborhood analysis identifies cell populations associated with phenotypes of interest from single-cell transcriptomics. *Nat. Biotechnol.* **40**, 355–363 (2022).

29. A. E. Pugh-Bernard, G. J. Silverman, A. J. Cappione, M. E. Villano, D. H. Ryan, R. A. Insel, I. Sanz, Regulation of inherently autoreactive VH4-34 B cells in the maintenance of human B cell tolerance. *J. Clin. Invest.* **108**, 1061–1070 (2001).

30. C. M. Tipton, C. F. Fucile, J. Darce, A. Chida, T. Ichikawa, I. Gregoretti, S. Schieferl, J. Hom, S. Jenks, R. J. Feldman, R. Mehr, C. Wei, F. E.-H. Lee, W. C. Cheung, A. F. Rosenberg, I. Sanz, Diversity, cellular origin and autoreactivity of antibody-secreting cell population expansions in acute systemic lupus erythematosus. *Nat. Immunol.* **16**, 755–765 (2015).

31. M. Ota, Y. Nagafuchi, H. Hatano, K. Ishigaki, C. Terao, Y. Takeshima, H. Yanaoka, S. Kobayashi, M. Okubo, H. Shirai, Y. Sugimori, J. Maeda, M. Nakano, S. Yamada, R. Yoshida, H. Tsuchiya, Y. Tsuchida, S. Akizuki, H. Yoshifuji, K. Ohmura, T. Mimori, K. Yoshida, D. Kurosaka, M. Okada, K. Setoguchi, H. Kaneko, N. Ban, N. Yabuki, K. Matsuki, H. Mutoh, S. Oyama, M. Okazaki, H. Tsunoda, Y. Iwasaki, S. Sumitomo, H. Shoda, Y. Kochi, Y. Okada, K. Yamamoto, T. Okamura, K. Fujio, Dynamic landscape of immune cell-specific gene regulation in immune-mediated diseases. *Cell* **184**, 3006-3021.e17 (2021).

32. D. Del Alcazar, Y. Wang, C. He, B. S. Wendel, P. M. Del Río-Estrada, J. Lin, Y. Ablanedo-Terrazas, M. J. Malone, S. M. Hernandez, I. Frank, A. Naji, G. Reyes-Terán, N. Jiang, L. F. Su, Mapping the lineage relationship between CXCR5+ and CXCR5- CD4+ T cells in HIV-infected human lymph nodes. *Cell Rep.* **28**, 3047-3060.e7 (2019).

33. G. Dunlap, A. Wagner, N. Meednu, R. Wang, F. Zhang, J. C. Ekabe, A. H. Jonsson, K. Wei, S. Sakaue, A. Nathan, V. P. Bykerk, L. T. Donlin, S. M. Goodman, G. S. Firestein, D. L. Boyle, V. M. Holers, L. W. Moreland, D. Tabechian, C. Pitzalis, A. Filer, S. Raychaudhuri, M. B. Brenner, J. Thakar, A. McDavid, D. A. Rao, J. H. Anolik, Clonal associations between lymphocyte subsets and functional states in rheumatoid arthritis synovium. *Nat. Commun.* **15**, 1–21 (2024).

34. K. E. Marks, D. A. Rao, T peripheral helper cells in autoimmune diseases. *Immunol. Rev.* **307**, 191–202 (2022).

35. M. Elahee, A. A. Mueller, R. Wang, K. E. Marks, T. Sasaki, Y. Cao, A. Fava, P. F. Dellaripa, F. Boin, D. A. Rao, A PD-1highCD4+ T cell population with a cytotoxic phenotype is associated with interstitial lung disease in systemic sclerosis. *ACR Open Rheumatol.* **6**, 429–439 (2024).

36. O. Khan, J. R. Giles, S. McDonald, S. Manne, S. F. Ngiow, K. P. Patel, M. T. Werner, A. C. Huang, K. A. Alexander, J. E. Wu, J. Attanasio, P. Yan, S. M. George, B. Bengsch, R. P. Staupe, G. Donahue, W. Xu, R. K. Amaravadi, X. Xu, G. C. Karakousis, T. C. Mitchell, L. M. Schuchter, J. Kaye, S. L. Berger, E. J. Wherry, TOX transcriptionally and epigenetically programs CD8+ T cell exhaustion. *Nature* **571**, 211–218 (2019).

37. A. C. Scott, F. Dündar, P. Zumbo, S. S. Chandran, C. A. Klebanoff, M. Shakiba, P. Trivedi, L. Menocal, H. Appleby, S. Camara, D. Zamarin, T. Walther, A. Snyder, M. R. Femia, E. A. Comen, H. Y. Wen, M. D. Hellmann, N. Anandasabapathy, Y. Liu, N. K. Altorki, P. Lauer, O. Levy, M. S. Glickman, J. Kaye, D. Betel, M. Philip, A. Schietinger, TOX is a critical regulator of tumour-specific T cell differentiation. *Nature* **571**, 270–274 (2019).

38. J. M. Odegard, B. R. Marks, L. D. DiPlacido, A. C. Poholek, D. H. Kono, C. Dong, R. A. Flavell, J. Craft, ICOS-dependent extrafollicular helper T cells elicit IgG production via IL-21 in systemic autoimmunity. *J. Exp. Med.* **205**, 2873–2886 (2008).

39. D. Vu Van, K. C. Beier, L.-J. Pietzke, M. S. Al Baz, R. K. Feist, S. Gurka, E. Hamelmann, R. A. Kroczek, A. Hutloff, Local T/B cooperation in inflamed tissues is supported by T follicular helper-like cells. *Nat. Commun.* **7**, 10875 (2016).

40. N. Swarnalekha, D. Schreiner, L. C. Litzler, S. Iftikhar, D. Kirchmeier, M. Künzli, Y. M. Son, J. Sun, E. A. Moreira, C. G. King, T resident helper cells promote humoral responses in the lung. *Sci. Immunol.* **6**, eabb6808 (2021).

41. Y. M. Son, I. S. Cheon, Y. Wu, C. Li, Z. Wang, X. Gao, Y. Chen, Y. Takahashi, Y.-X. Fu, A. L. Dent, M. H. Kaplan, J. J. Taylor, W. Cui, J. Sun, Tissue-resident CD4+ T helper cells assist the development of protective respiratory B and CD8+ T cell memory responses. *Sci. Immunol.* **6**, eabb6852 (2021).

42. W. Xu, X. Zhao, X. Wang, H. Feng, M. Gou, W. Jin, X. Wang, X. Liu, C. Dong, The transcription factor Tox2 drives T follicular helper cell development via regulating chromatin accessibility. *Immunity* **51**, 826-839.e5 (2019).

43. C. Law, V. S. Wacleche, Y. Cao, A. Pillai, J. Sowerby, B. Hancock, A. Horisberger, S. Bracero, V. Skidanova, Z. Li, I. Adejoorin, E. Dillon, I. J. Benque, D. P. Nunez, D. P. Simmons, J. Keegan, L. Chen, T. Baker, P. Z. Brohawn, H. Al-Mossawi, L.-Y. Hao, B. Jones, N. Rao, Y. Qu, S. E. Alves, Accelerating

Medicines Partnership: RA/SLE Network, A. H. Jonsson, K. S. Shaw, R. A. Vleugels, E. Massarotti, K. H. Costenbader, M. B. Brenner, J. A. Lederer, J. F. Hultquist, J. Choi, D. A. Rao, Interferon subverts an AHR-JUN axis to promote CXCL13+ T cells in lupus. *Nature* **631**, 857–866 (2024).

44. K. Hatzi, J. P. Nance, M. A. Kroenke, M. Bothwell, E. K. Haddad, A. Melnick, S. Crotty, BCL6 orchestrates Tfh cell differentiation via multiple distinct mechanisms. *J. Exp. Med.* **212**, 539–553 (2015).

45. J. Choi, H. Diao, C. E. Faliti, J. Truong, M. Rossi, S. Bélanger, B. Yu, A. W. Goldrath, M. E. Pipkin, S. Crotty, Bcl-6 is the nexus transcription factor of T follicular helper cells via repressor-of-repressor circuits. *Nat. Immunol.* **21**, 777–789 (2020).

46. M. A. Kroenke, D. Eto, M. Locci, M. Cho, T. Davidson, E. K. Haddad, S. Crotty, Bcl6 and Maf cooperate to instruct human follicular helper CD4 T cell differentiation. *J. Immunol.* **188**, 3734–3744 (2012).

47. M. Seyedsadr, M. F. Bang, E. C. McCarthy, S. Zhang, H.-C. Chen, M. Mohebbi, W. Hugo, J. K. Whitmire, M. G. Lechner, M. A. Su, A pathologically expanded, clonal lineage of IL-21-producing CD4+ T cells drives inflammatory neuropathy. *J. Clin. Invest.* **134** (2024).

48. D. Baumjohann, T. Okada, K. M. Ansel, Cutting Edge: Distinct waves of BCL6 expression during T follicular helper cell development. *J. Immunol.* **187**, 2089–2092 (2011).

49. M. C. Hochberg, Updating the American College of Rheumatology revised criteria for the classification of systemic lupus erythematosus. *Arthritis Rheum.* **40**, 1725 (1997).

50. M. Petri, A.-M. Orbai, G. S. Alarcón, C. Gordon, J. T. Merrill, P. R. Fortin, I. N. Bruce, D. Isenberg, D. J. Wallace, O. Nived, G. Sturfelt, R. Ramsey-Goldman, S.-C. Bae, J. G. Hanly, J. Sánchez-Guerrero, A. Clarke, C. Aranow, S. Manzi, M. Urowitz, D. Gladman, K. Kalunian, M. Costner, V. P. Werth, A. Zoma, S. Bernatsky, G. Ruiz-Irastorza, M. A. Khamashta, S. Jacobsen, J. P. Buyon, P. Maddison, M. A. Dooley, R. F. van Vollenhoven, E. Ginzler, T. Stoll, C. Peschken, J. L. Jorizzo, J. P. Callen, S. S. Lim, B. J. Fessler, M. Inanc, D. L. Kamen, A. Rahman, K. Steinsson, A. G. Franks Jr, L. Sigler, S. Hameed, H. Fang, N. Pham, R. Brey, M. H. Weisman, G. McGwin Jr, L. S. Magder, Derivation and validation of the Systemic Lupus International Collaborating Clinics classification criteria for systemic lupus erythematosus. *Arthritis Rheum.* **64**, 2677–2686 (2012).

51. M. Aringer, K. Costenbader, D. Daikh, R. Brinks, M. Mosca, R. Ramsey-Goldman, J. S. Smolen, D. Wofsy, D. T. Boumpas, D. L. Kamen, D. Jayne, R. Cervera, N. Costedoat-Chalumeau, B. Diamond, D. D. Gladman, B. Hahn, F. Hiepe, S. Jacobsen, D. Khanna, K. Lerstrøm, E. Massarotti, J. McCune, G. Ruiz-Irastorza, J. Sanchez-Guerrero, M. Schneider, M. Urowitz, G. Bertsias, B. F. Hoyer, N. Leuchten, C. Tani, S. K. Tedeschi, Z. Touma, G. Schmajuk, B. Anic, F. Assan, T. M. Chan, A. E. Clarke, M. K. Crow, L. Czirják, A. Doria, W. Graninger, B. Halda-Kiss, S. Hasni, P. M. Izmirly, M. Jung, G. Kumánovics, X. Mariette, I. Padjen, J. M. Pego-Reigosa, J. Romero-Diaz, Í. Rúa-Figueroa Fernández, R. Seror, G. H. Stummvoll, Y. Tanaka, M. G. Tektonidou, C. Vasconcelos, E. M. Vital, D. J. Wallace, S. Yavuz, P. L. Meroni, M. J. Fritzler, R. Naden, T. Dörner, S. R. Johnson, 2019 European League Against Rheumatism/American College of Rheumatology classification criteria for systemic lupus erythematosus. *Arthritis Rheumatol.* **71**, 1400–1412 (2019).

52. Y. Hao, T. Stuart, M. H. Kowalski, S. Choudhary, P. Hoffman, A. Hartman, A. Srivastava, G. Molla, S. Madad, C. Fernandez-Granda, R. Satija, Dictionary learning for integrative, multimodal and scalable single-cell analysis. *Nat. Biotechnol.* **42**, 293–304 (2024).

53. N. Borcherding, N. L. Bormann, scRepertoire: An R-based toolkit for single-cell immune receptor analysis. *F1000Res.* **9**, 47 (2020).

Figure 1

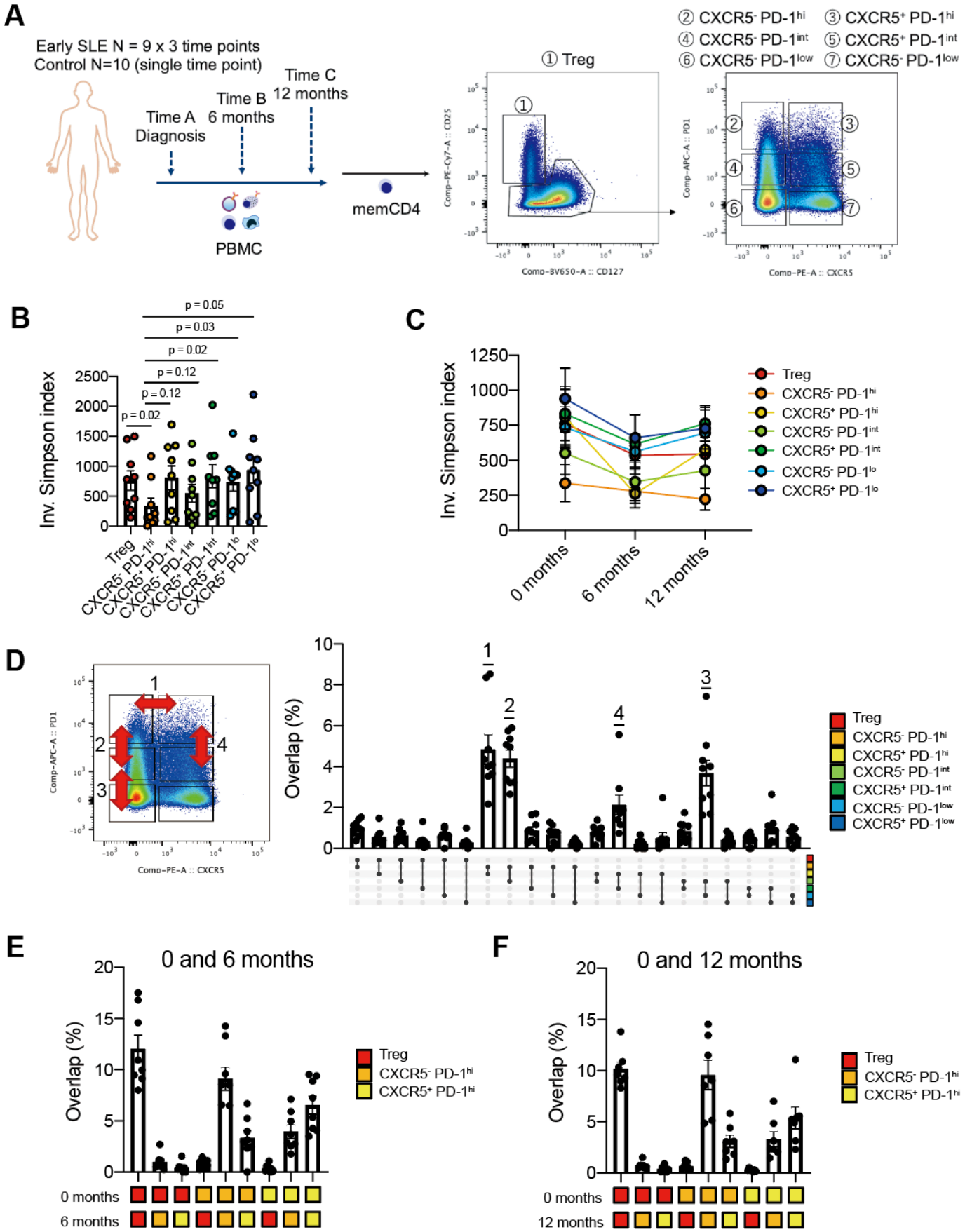
A
Early SLE N = 9 x 3 time points
Control N=10 (single time point)
Time A
Diagnosis
Time B
6 months
Time C
12 months
PBMC
memCD4
① Treg
② CXCR5⁻ PD-1hi
③ CXCR5⁺ PD-1hi
④ CXCR5⁻ PD-1int
⑤ CXCR5⁺ PD-1int
⑥ CXCR5⁻ PD-1low
⑦ CXCR5⁻ PD-1low
Comp-PE-Cy7-A :: CD25
Comp-BV650-A :: CD127
Comp-APC-A :: PD1
Comp-PE-A :: CXCR5
B
Inv. Simpson index
p = 0.05
p = 0.03
p = 0.02
p = 0.12
p = 0.12
p = 0.02
Treg
CXCR5⁻ PD-1hi
CXCR5⁺ PD-1hi
CXCR5⁻ PD-1int
CXCR5⁺ PD-1int
CXCR5⁻ PD-1lo
CXCR5⁺ PD-1lo
C
Inv. Simpson index
0 months
6 months
12 months
D
Overlap (%)
E
0 and 6 months
Overlap (%)
0 months
6 months
F
0 and 12 months
Overlap (%)
0 months
12 months

Figure 2

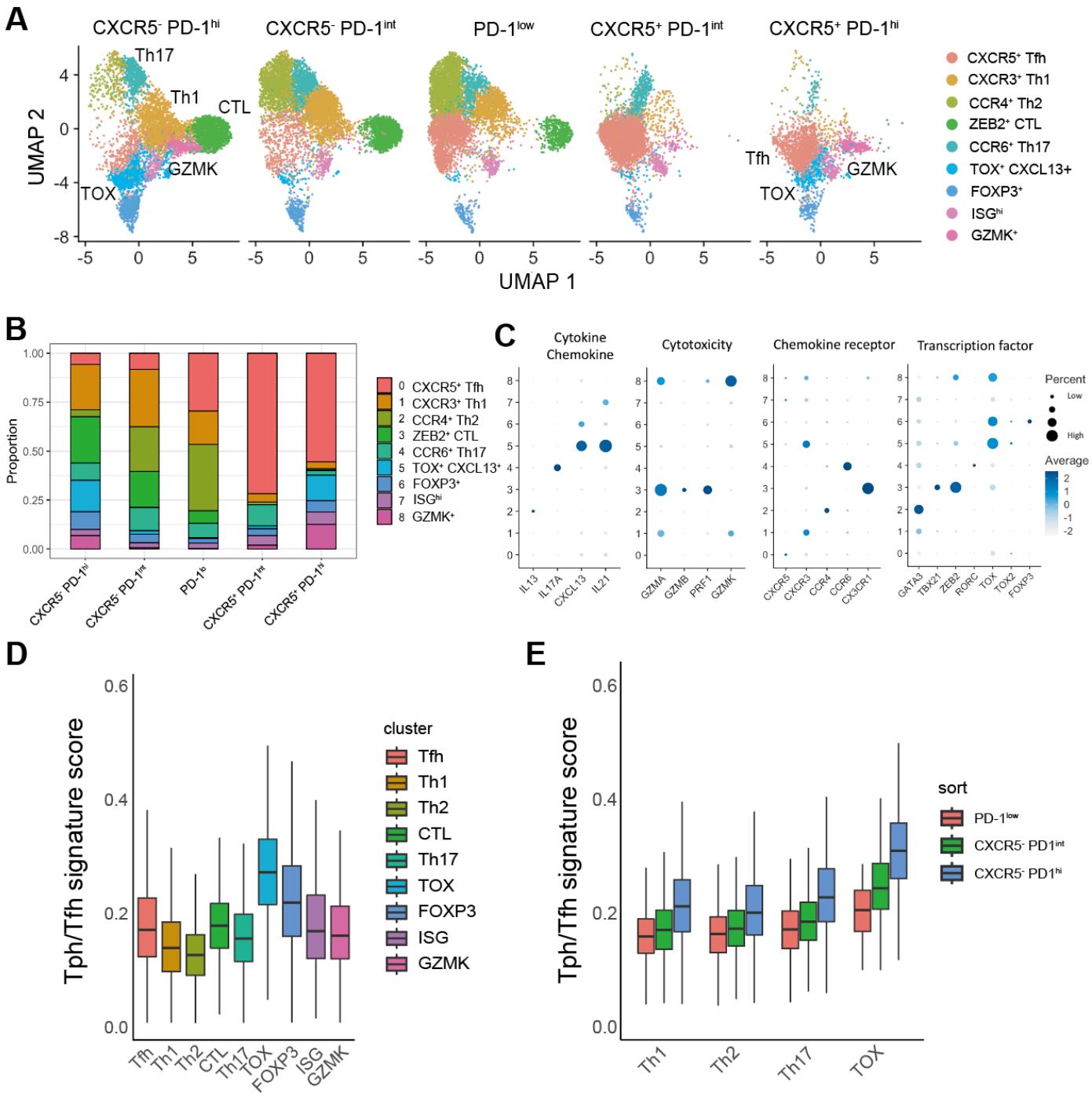
A
CXCR5- PD-1hi
CXCR5- PD-1int
PD-1low
CXCR5+ PD-1int
CXCR5+ PD-1hi
Th17
Th1
CTL
GZMK
TOX
Tfh
UMAP 2
UMAP 1
CXCR5+ Tfh
CXCR3+ Th1
CCR4+ Th2
ZEB2+ CTL
CCR6+ Th17
TOX+ CXCL13+
FOXP3+
ISGhi
GZMK+
B
Proportion
0 CXCR5+ Tfh
1 CXCR3+ Th1
2 CCR4+ Th2
3 ZEB2+ CTL
4 CCR6+ Th17
5 TOX+ CXCL13+
6 FOXP3+
7 ISGhi
8 GZMK+
C
Cytokine Chemokine
Cytotoxicity
Chemokine receptor
Transcription factor
IL13
IL17A
CXCL13
IL21
GZMA
GZMB
PRF1
GZMK
CXCR5
CXCR3
CCR4
CCR6
CX3CR1
GATA3
TBX21
ZEB2
RORC
TOX
TOX2
FOXP3
Percent
Low
High
Average
D
Tph/Tfh signature score
cluster
Tfh
Th1
Th2
CTL
Th17
TOX
FOXP3
ISG
GZMK
E
Tph/Tfh signature score
sort
PD-1low
CXCR5- PD1int
CXCR5- PD1hi
Th1
Th2
Th17
TOX

Figure 3

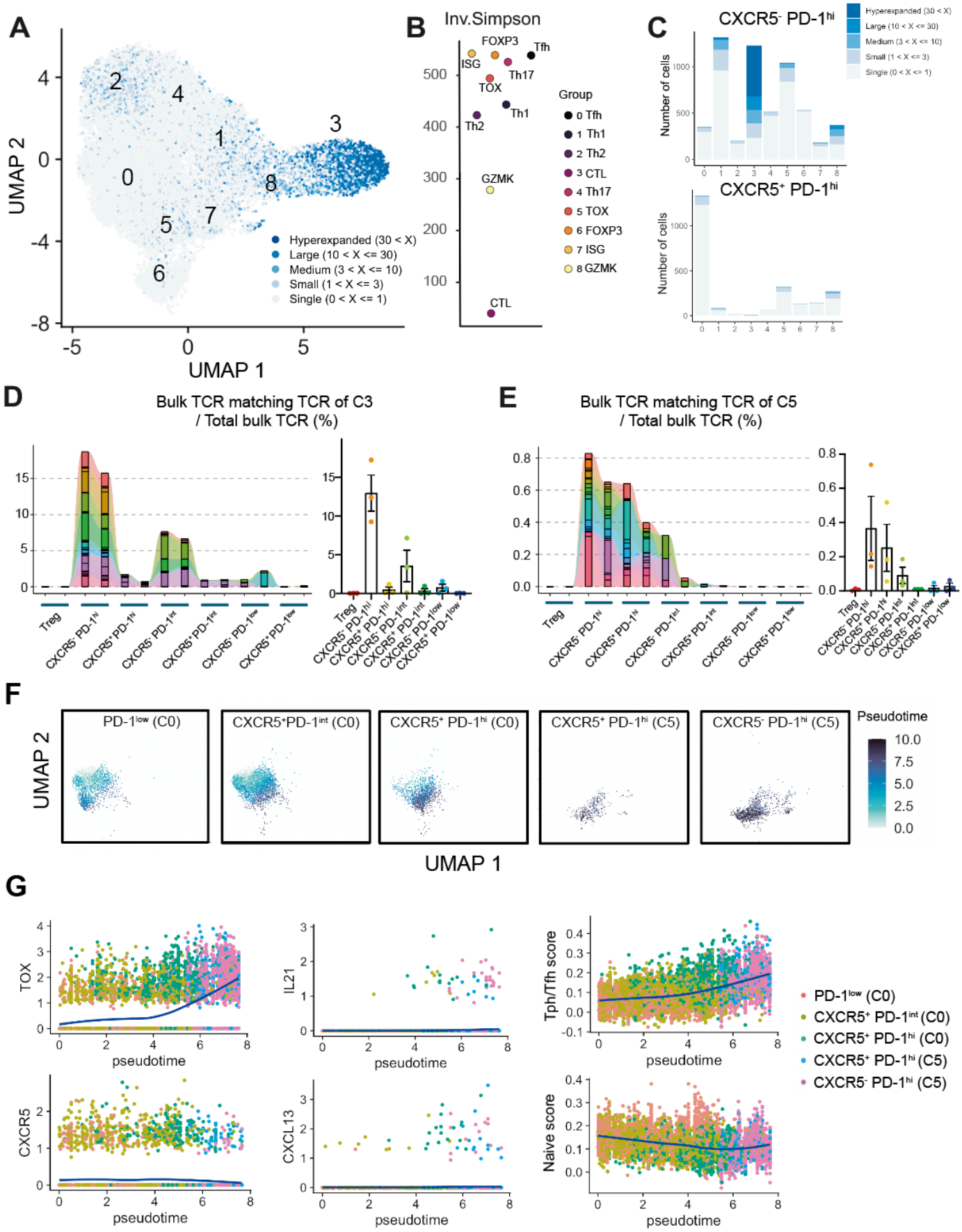
A
UMAP 2
UMAP 1
Hyperexpanded (30 < X)
Large (10 < X <= 30)
Medium (3 < X <= 10)
Small (1 < X <= 3)
Single (0 < X <= 1)
B
Inv.Simpson
FOXP3
Tfh
ISG
Th17
TOX
Th1
Th2
GZMK
CTL
Group
0 Tfh
1 Th1
2 Th2
3 CTL
4 Th17
5 TOX
6 FOXP3
7 ISG
8 GZMK
C
CXCR5- PD-1hi
CXCR5+ PD-1hi
Number of cells
D
Bulk TCR matching TCR of C3 / Total bulk TCR (%)
E
Bulk TCR matching TCR of C5 / Total bulk TCR (%)
Treg
CXCR5- PD-1hi
CXCR5+ PD-1hi
CXCR5- PD-1int
CXCR5+ PD-1int
CXCR5- PD-1low
CXCR5+ PD-1low
F
PD-1low (C0)
CXCR5+PD-1int (C0)
CXCR5+ PD-1hi (C0)
CXCR5+ PD-1hi (C5)
CXCR5- PD-1hi (C5)
Pseudotime
UMAP 2
UMAP 1
G
TOX
IL21
Tph/Tfh score
CXCR5
CXCL13
Naive score
pseudotime
PD-1low (C0)
CXCR5+ PD-1int (C0)
CXCR5+ PD-1hi (C0)
CXCR5+ PD-1hi (C5)
CXCR5- PD-1hi (C5)

Figure 4

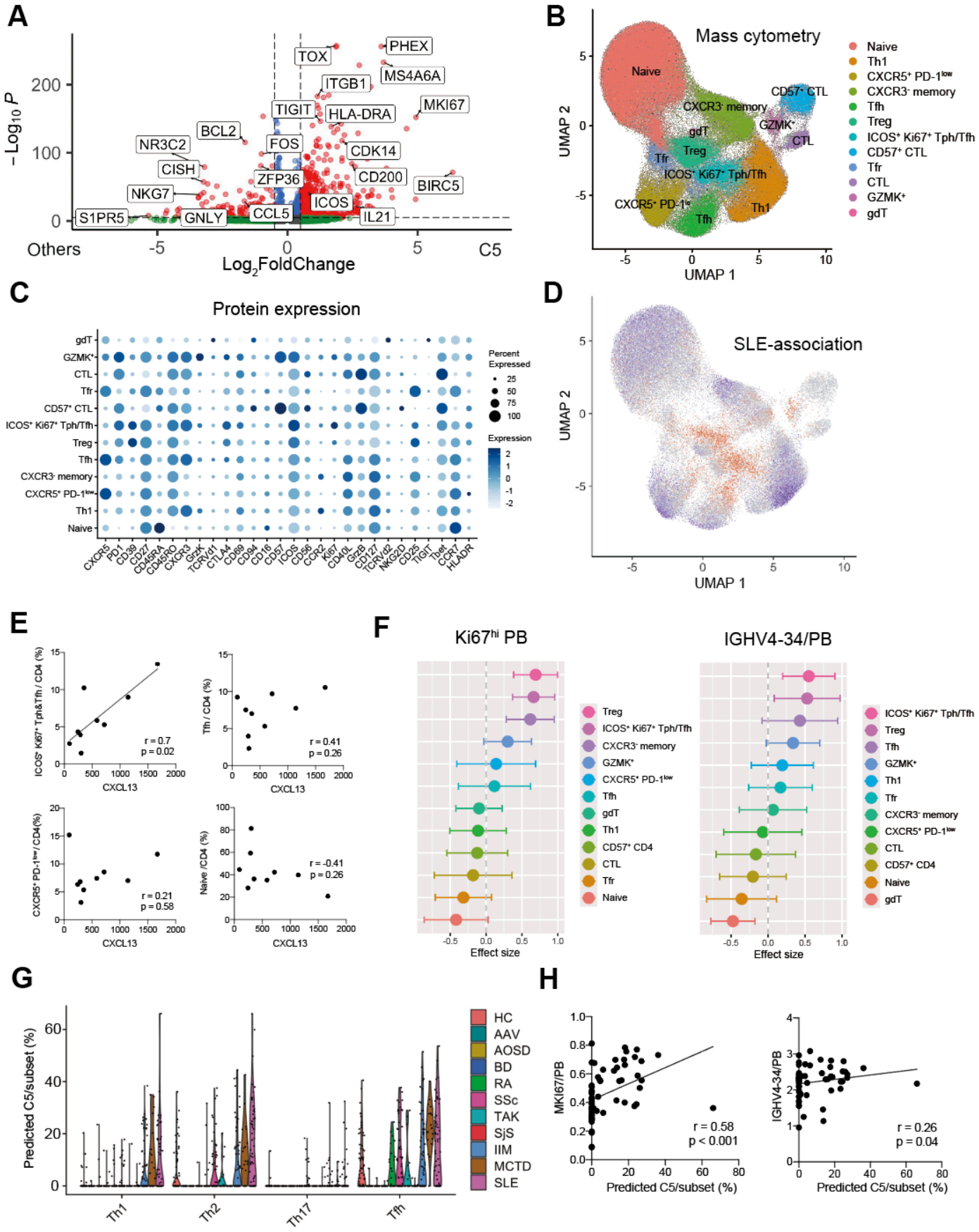
A
PHEX
TOX
MS4A6A
ITGB1
MKI67
TIGIT
HLA-DRA
BCL2
NR3C2
FOS
CDK14
CISH
ZFP36
CD200
BIRC5
NKG7
ICOS
S1PR5
GNLY
CCL5
IL21
Others
C5
Log2FoldChange
−Log10 P
B
Mass cytometry
Naive
CD57+ CTL
CXCR3- memory
GZMK+
gdT
CTL
Treg
Tfr
ICOS+ Ki67+ Tph/Tfh
CXCR5+ PD-1low
Th1
Tfh
UMAP 1
UMAP 2
C
Protein expression
Percent Expressed
Expression
D
SLE-association
E
ICOS+ Ki67+ Tph&Tfh / CD4 (%)
Tfh / CD4 (%)
CXCR5+ PD-1low / CD4(%)
Naive /CD4 (%)
CXCL13
r = 0.7
p = 0.02
r = 0.41
p = 0.26
r = 0.21
p = 0.58
r = -0.41
p = 0.26
F
Ki67hi PB
IGHV4-34/PB
Effect size
G
Predicted C5/subset (%)
HC
AAV
AOSD
BD
RA
SSc
TAK
SjS
IIM
MCTD
SLE
Th1
Th2
Th17
Tfh
H
MKI67/PB
IGHV4-34/PB
Predicted C5/subset (%)
r = 0.58
p < 0.001
r = 0.26
p = 0.04

Figure 5

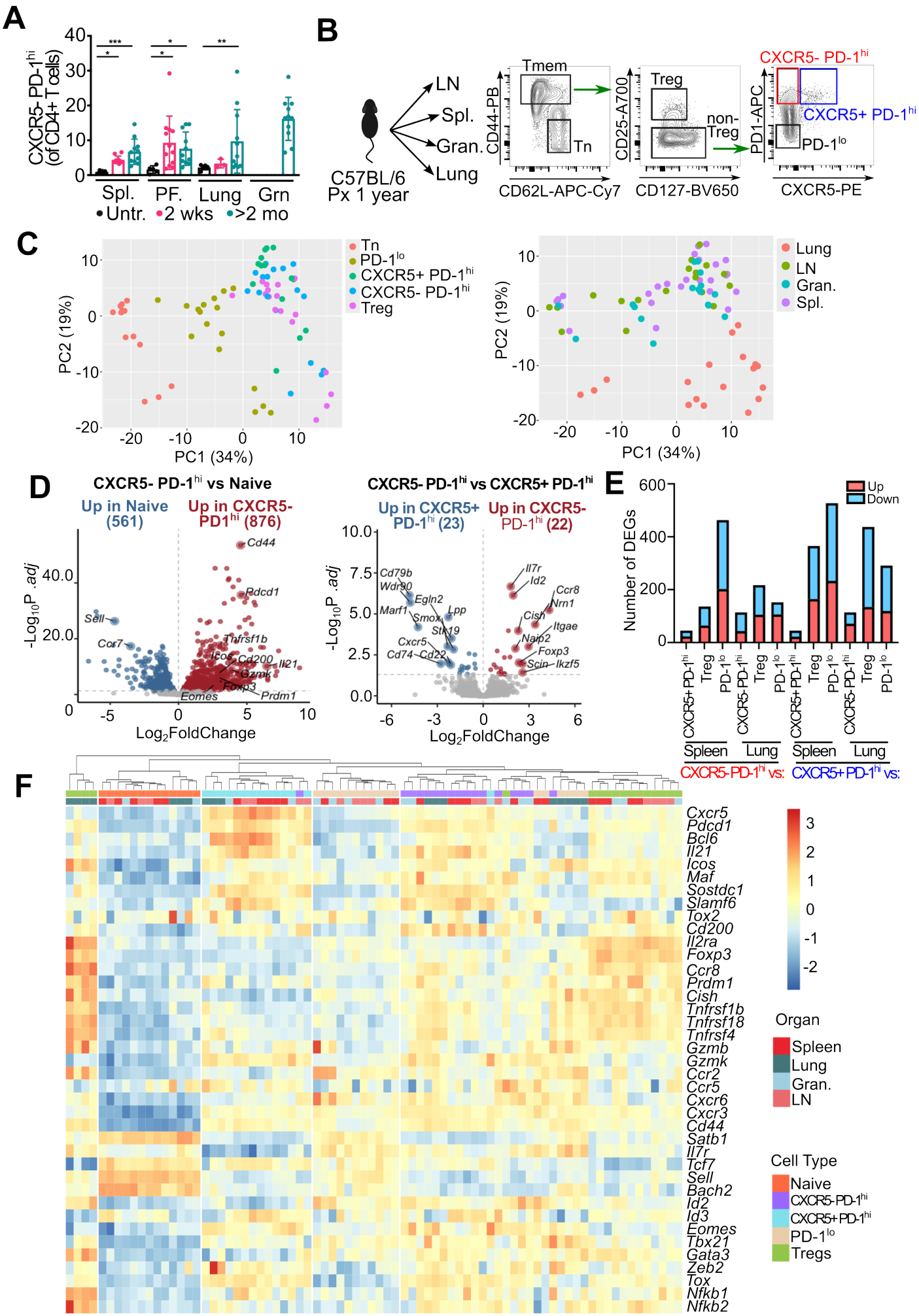
A
CXCR5- PD-1hi (of CD4+ T cells)
Spl.
PF.
Lung
Grn
Untr.
2 wks
>2 mo
B
C57BL/6
Px 1 year
LN
Spl.
Gran.
Lung
Tmem
Tn
CD44-PB
CD62L-APC-Cy7
Treg
non-Treg
CD25-A700
CD127-BV650
CXCR5- PD-1hi
CXCR5+ PD-1hi
PD-1lo
PD1-APC
CXCR5-PE
C
Tn
PD-1lo
CXCR5+ PD-1hi
CXCR5- PD-1hi
Treg
PC1 (34%)
PC2 (19%)
Lung
LN
Gran.
Spl.
D
CXCR5- PD-1hi vs Naive
Up in Naive (561)
Up in CXCR5- PD1hi (876)
Cd44
Pdcd1
Sell
Ccr7
Tnfrsf1b
Icos
Cd200
Il21
Gzmk
Foxp3
Eomes
Prdm1
-Log10P .adj
Log2FoldChange
CXCR5- PD-1hi vs CXCR5+ PD-1hi
Up in CXCR5+ PD-1hi (23)
Up in CXCR5- PD-1hi (22)
Cd79b
Wdr90
Egln2
Marf1
Smox
Lpp
Stk19
Cxcr5
Cd74
Cd22
Il7r
Id2
Ccr8
Nrn1
Cish
Itgae
Naip2
Foxp3
Scin
Ikzf5
E
Number of DEGs
Up
Down
CXCR5+ PD-1hi
Treg
PD-1lo
CXCR5- PD-1hi
Spleen
Lung
CXCR5- PD-1hi vs:
CXCR5+ PD-1hi vs:
F
Cxcr5
Pdcd1
Bcl6
Il21
Icos
Maf
Sostdc1
Slamf6
Tox2
Cd200
Il2ra
Foxp3
Ccr8
Prdm1
Cish
Tnfrsf1b
Tnfrsf18
Tnfrsf4
Gzmb
Gzmk
Ccr2
Ccr5
Cxcr6
Cxcr3
Cd44
Satb1
Il7r
Tcf7
Sell
Bach2
Id2
Id3
Eomes
Tbx21
Gata3
Zeb2
Tox
Nfkb1
Nfkb2
Organ
Spleen
Lung
Gran.
LN
Cell Type
Naive
CXCR5- PD-1hi
CXCR5+ PD-1hi
PD-1lo
Tregs

Figure 6

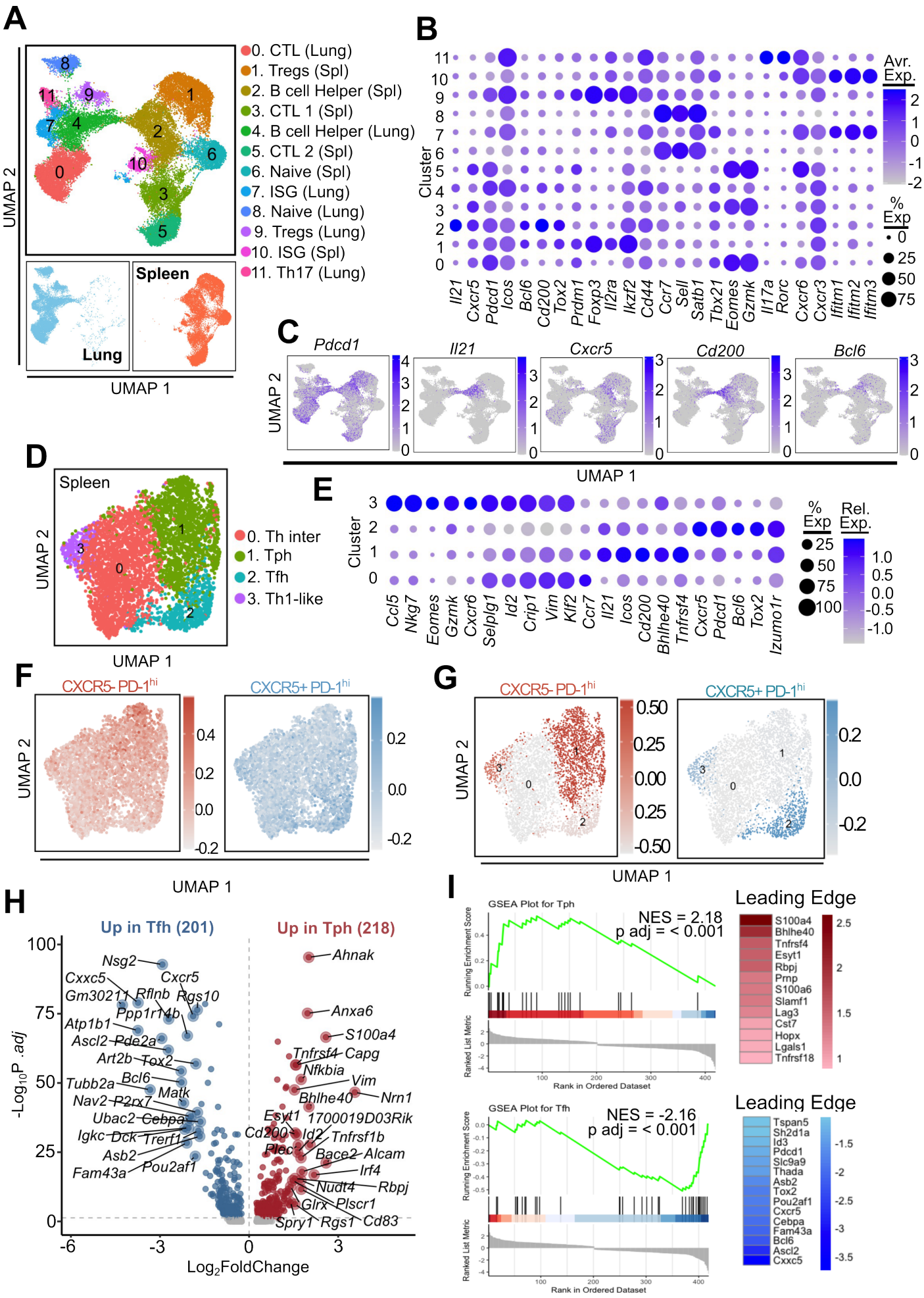
A
0. CTL (Lung)
1. Tregs (Spl)
2. B cell Helper (Spl)
3. CTL 1 (Spl)
4. B cell Helper (Lung)
5. CTL 2 (Spl)
6. Naive (Spl)
7. ISG (Lung)
8. Naive (Lung)
9. Tregs (Lung)
10. ISG (Spl)
11. Th17 (Lung)
Lung
Spleen
UMAP 1
UMAP 2
B
Cluster
Avr. Exp.
% Exp
Il21 Cxcr5 Pdcd1 Icos Bcl6 Cd200 Tox2 Prdm1 Foxp3 Il2ra Ikzf2 Cd44 Ccr7 Sell Satb1 Tbx21 Eomes Gzmk Il17a Rorc Cxcr6 Cxcr3 Ifitm1 Ifitm2 Ifitm3
C
Pdcd1 Il21 Cxcr5 Cd200 Bcl6
UMAP 1
UMAP 2
D
Spleen
0. Th inter
1. Tph
2. Tfh
3. Th1-like
UMAP 1
UMAP 2
E
Cluster
% Exp
Rel. Exp.
Ccl5 Nkg7 Eomes Gzmk Cxcr6 Selplg1 Id2 Crip1 Vim Klf2 Ccr7 Il21 Icos Cd200 Bhlhe40 Tnfrsf4 Cxcr5 Pdcd1 Bcl6 Tox2 Izumo1r
F
CXCR5- PD-1hi
CXCR5+ PD-1hi
UMAP 1
UMAP 2
G
CXCR5- PD-1hi
CXCR5+ PD-1hi
UMAP 1
UMAP 2
H
Up in Tfh (201)
Up in Tph (218)
Nsg2 Cxxc5 Cxcr5 Gm30211 Rflnb Rgs10 Ppp1r14b Atp1b1 Ascl2 Pde2a Art2b Tox2 Tubb2a Bcl6 Matk Nav2 P2rx7 Ubac2 Cebpa Igkc Dck Trerf1 Asb2 Fam43a Pou2af1
Ahnak Anxa6 S100a4 Tnfrsf4 Capg Nfkbia Vim Bhlhe40 Nrn1 Esyt1 1700019D03Rik Cd200 Id2 Tnfrsf1b Plac8 Bace2 Alcam Irf4 Nudt4 Rbpj Glrx Plscr1 Spry1 Rgs1 Cd83
-Log10P .adj
Log2FoldChange
I
GSEA Plot for Tph
NES = 2.18
p adj = < 0.001
Leading Edge
S100a4 Bhlhe40 Tnfrsf4 Esyt1 Rbpj Prnp S100a6 Slamf1 Lag3 Cst7 Hopx Lgals1 Tnfrsf18
GSEA Plot for Tfh
NES = -2.16
p adj = < 0.001
Leading Edge
Tspan5 Sh2d1a Id3 Pdcd1 Slc9a9 Thada Asb2 Tox2 Pou2af1 Cxcr5 Cebpa Fam43a Bcl6 Ascl2 Cxxc5
Running Enrichment Score
Ranked List Metric
Rank in Ordered Dataset

Figure 7

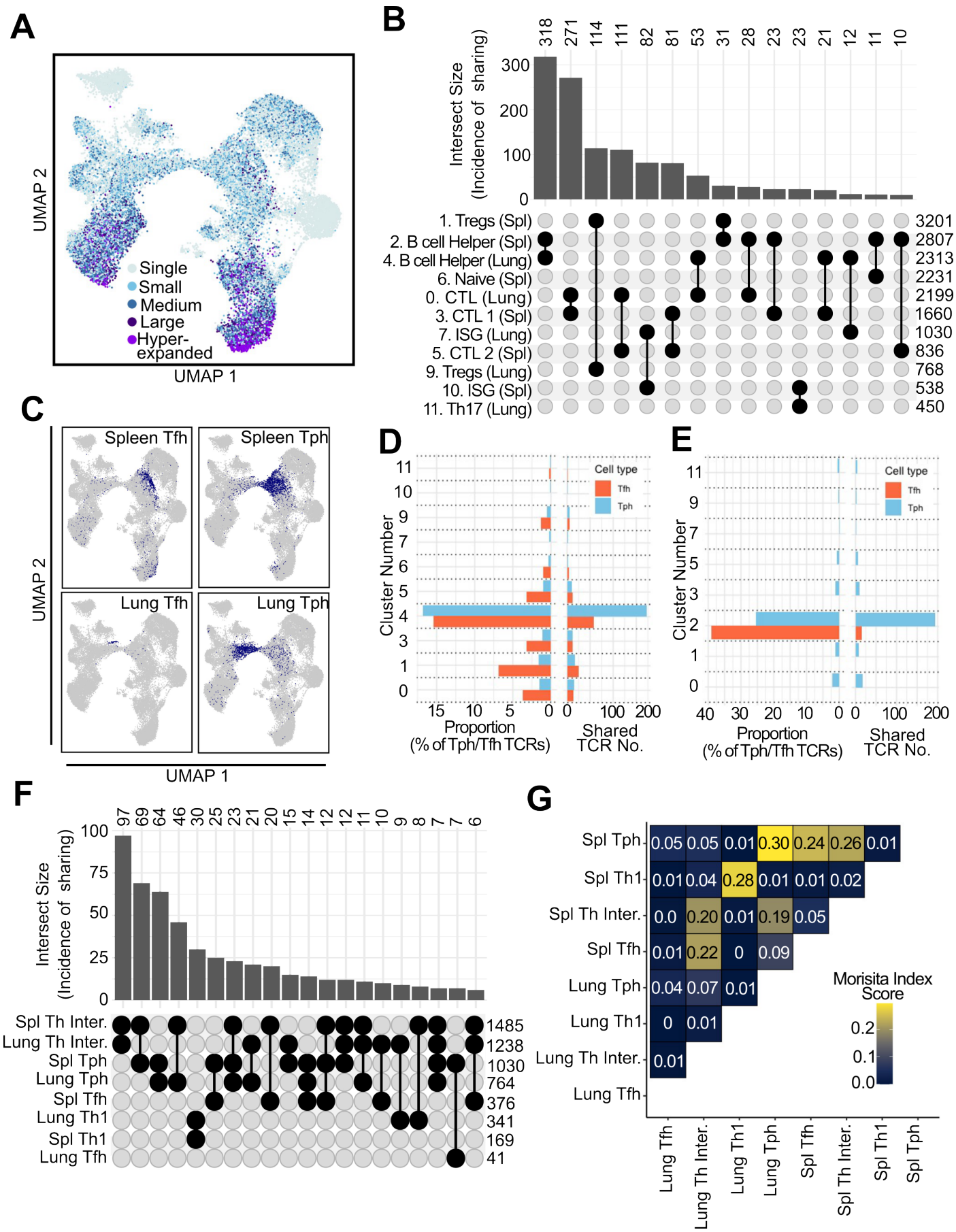
A
UMAP 2
UMAP 1
Single
Small
Medium
Large
Hyper-expanded
B
Intersect Size (Incidence of sharing)
318 271 114 111 82 81 53 31 28 23 23 21 12 11 10
1. Tregs (Spl) 3201
2. B cell Helper (Spl) 2807
4. B cell Helper (Lung) 2313
6. Naive (Spl) 2231
0. CTL (Lung) 2199
3. CTL 1 (Spl) 1660
7. ISG (Lung) 1030
5. CTL 2 (Spl) 836
9. Tregs (Lung) 768
10. ISG (Spl) 538
11. Th17 (Lung) 450
C
Spleen Tfh
Spleen Tph
Lung Tfh
Lung Tph
D
Cell type
Tfh
Tph
Cluster Number
Proportion (% of Tph/Tfh TCRs)
Shared TCR No.
E
F
97 69 64 46 30 25 23 21 20 15 14 12 12 11 10 9 8 7 7 6
Spl Th Inter. 1485
Lung Th Inter. 1238
Spl Tph 1030
Lung Tph 764
Spl Tfh 376
Lung Th1 341
Spl Th1 169
Lung Tfh 41
G
Morisita Index Score
Spl Tph 0.05 0.05 0.01 0.30 0.24 0.26 0.01
Spl Th1 0.01 0.04 0.28 0.01 0.01 0.02
Spl Th Inter. 0.0 0.20 0.01 0.19 0.05
Spl Tfh 0.01 0.22 0 0.09
Lung Tph 0.04 0.07 0.01
Lung Th1 0 0.01
Lung Th Inter. 0.01
Lung Tfh

Figure 8

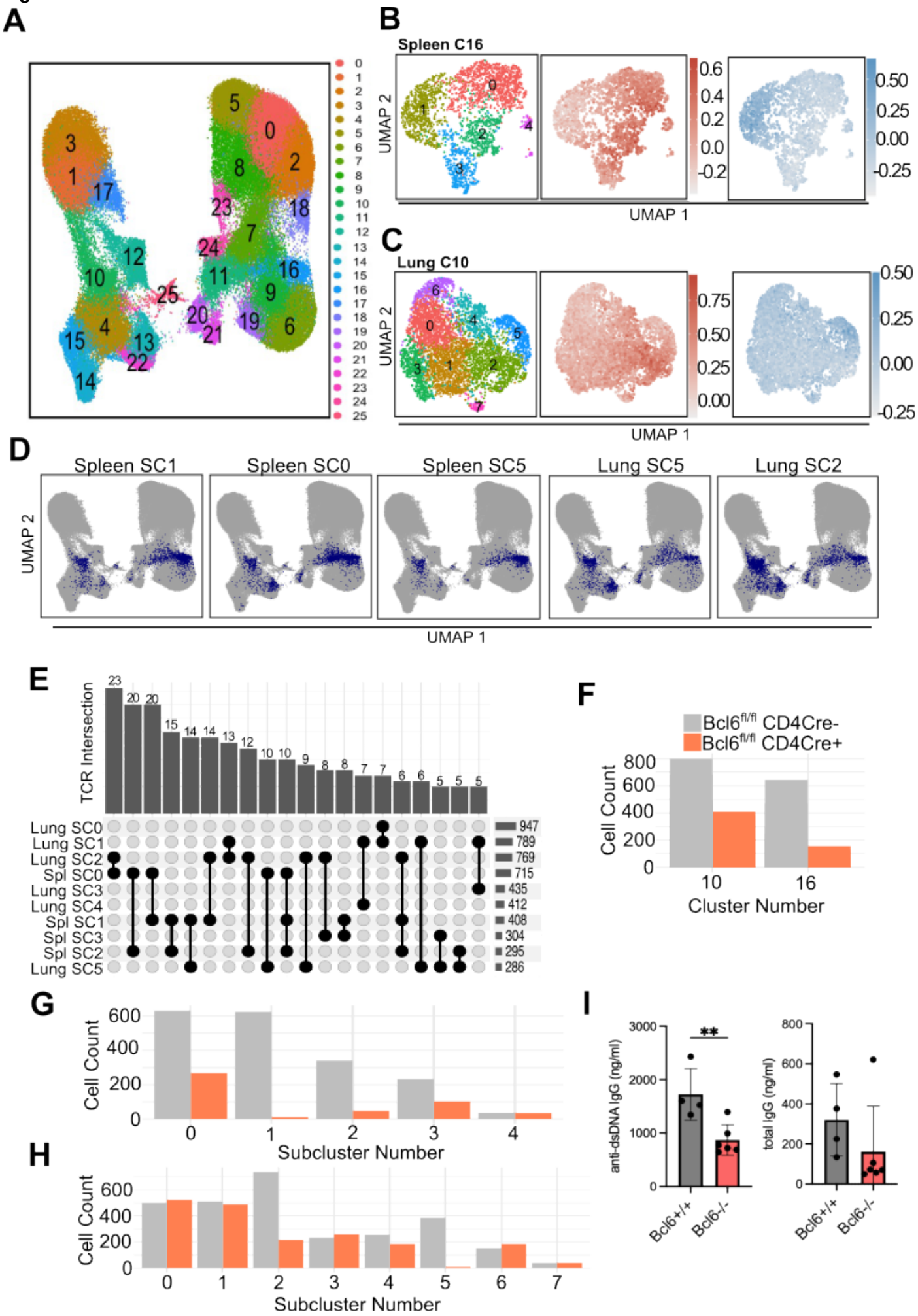
A
B
Spleen C16
UMAP 2
UMAP 1
C
Lung C10
UMAP 2
UMAP 1
D
Spleen SC1
Spleen SC0
Spleen SC5
Lung SC5
Lung SC2
UMAP 2
UMAP 1
E
TCR Intersection
Lung SC0
Lung SC1
Lung SC2
Spl SC0
Lung SC3
Lung SC4
Spl SC1
Spl SC3
Spl SC2
Lung SC5
F
Bcl6fl/fl CD4Cre-
Bcl6fl/fl CD4Cre+
Cell Count
Cluster Number
G
Cell Count
Subcluster Number
H
Cell Count
Subcluster Number
I
anti-dsDNA IgG (ng/ml)
total IgG (ng/ml)
Bcl6+/+
Bcl6-/-

Supplementary Figure 1

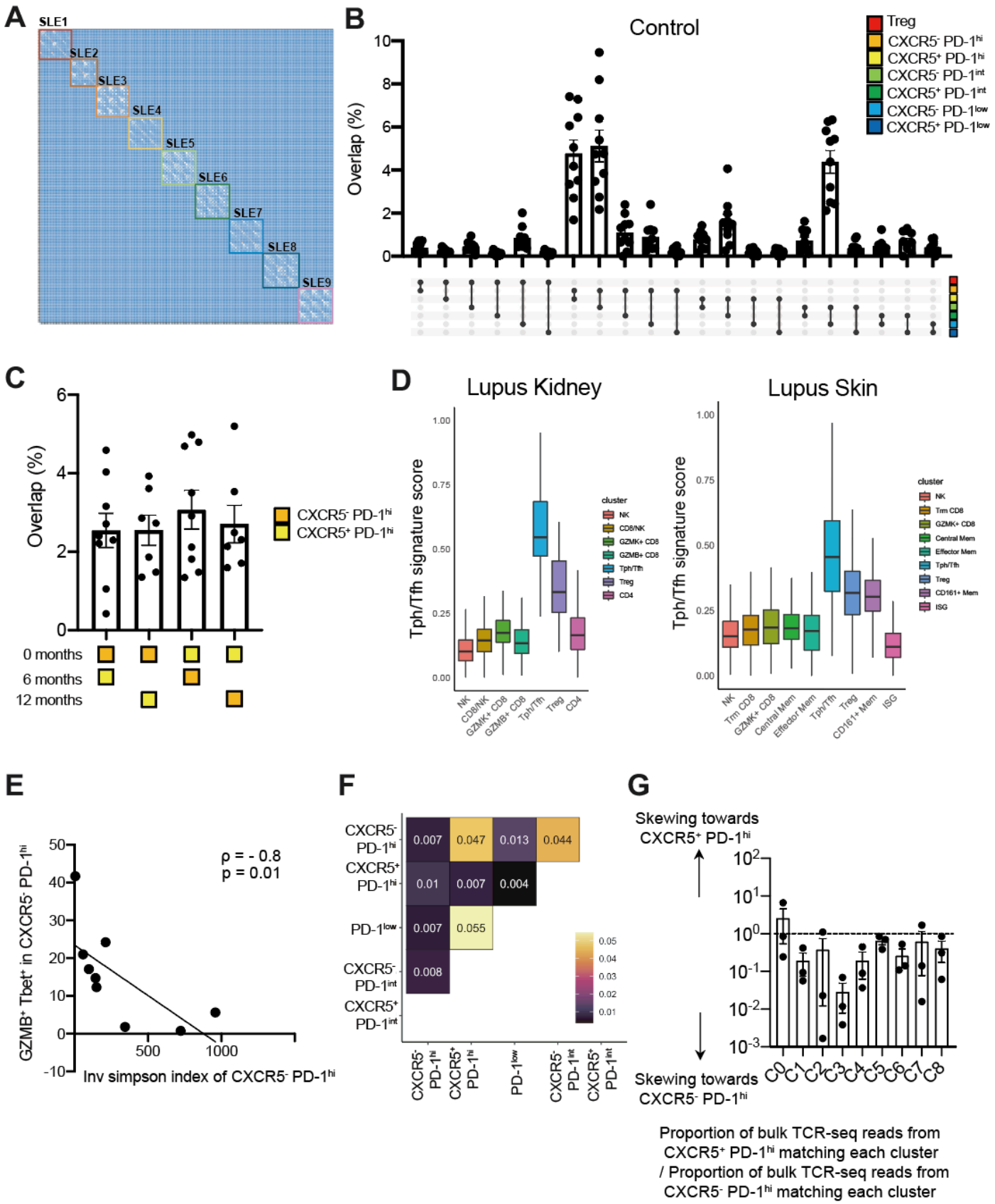

Supplementary Figure 2

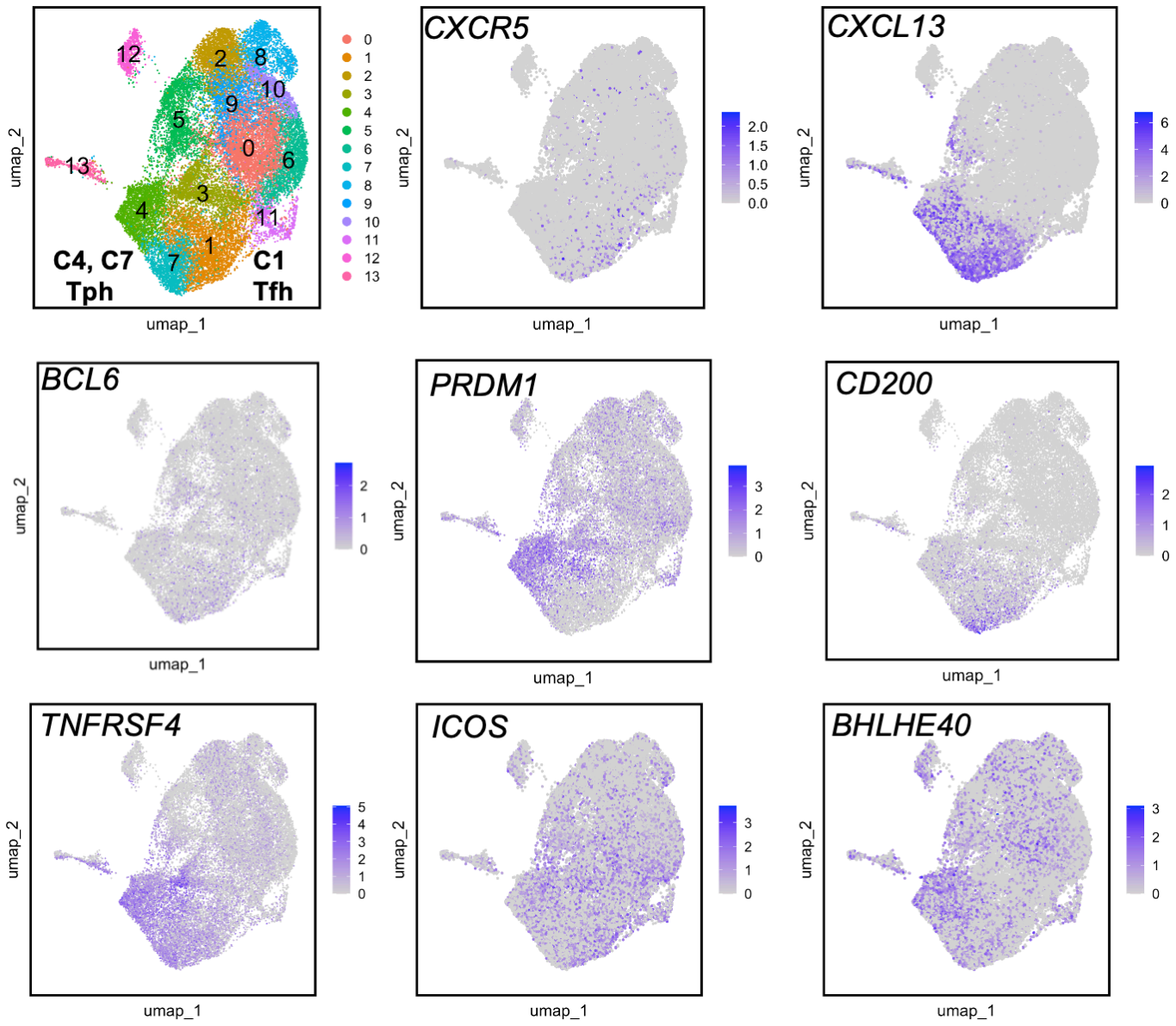

Supplementary Figure 3

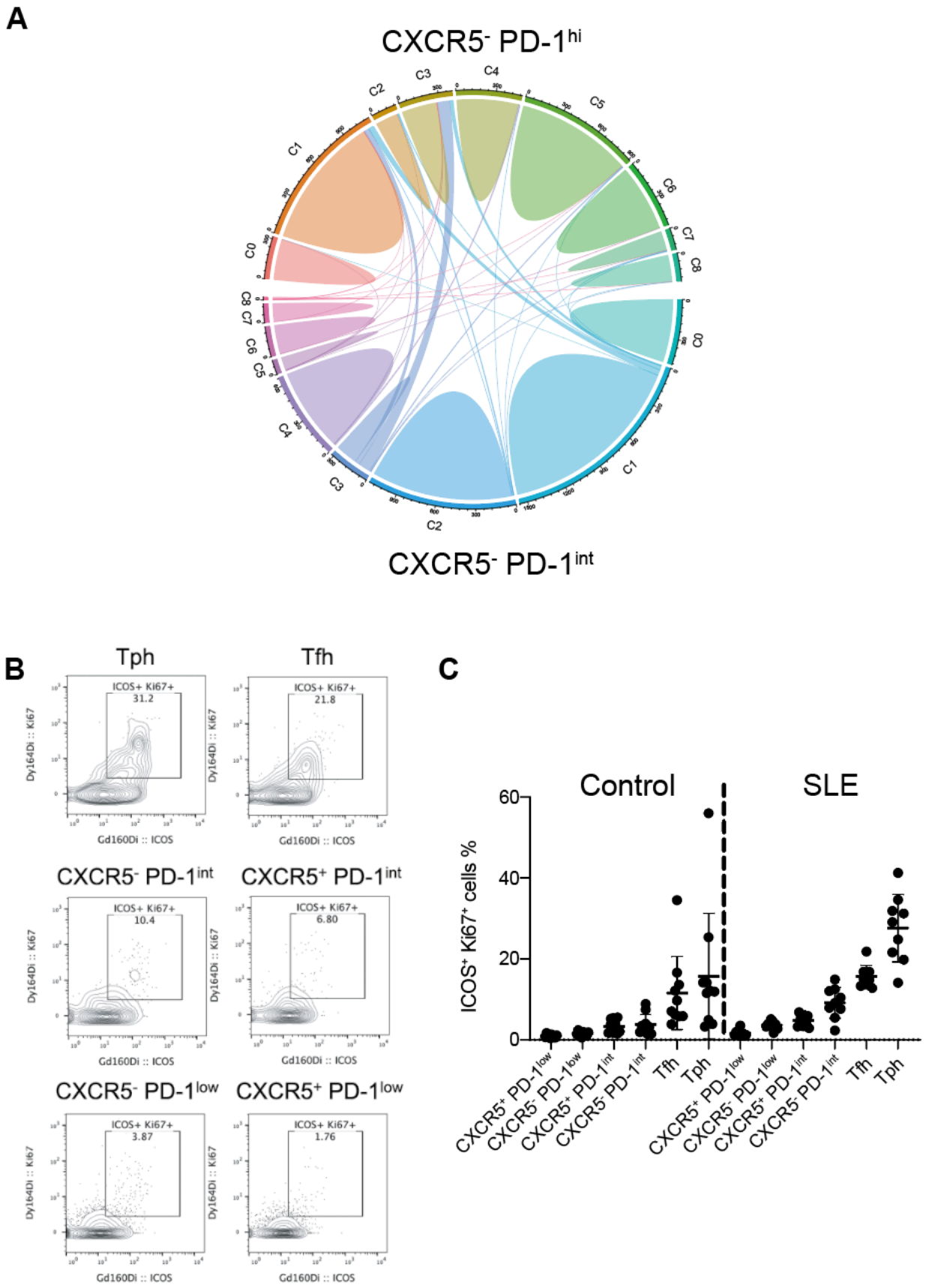

Supplementary Figure 4

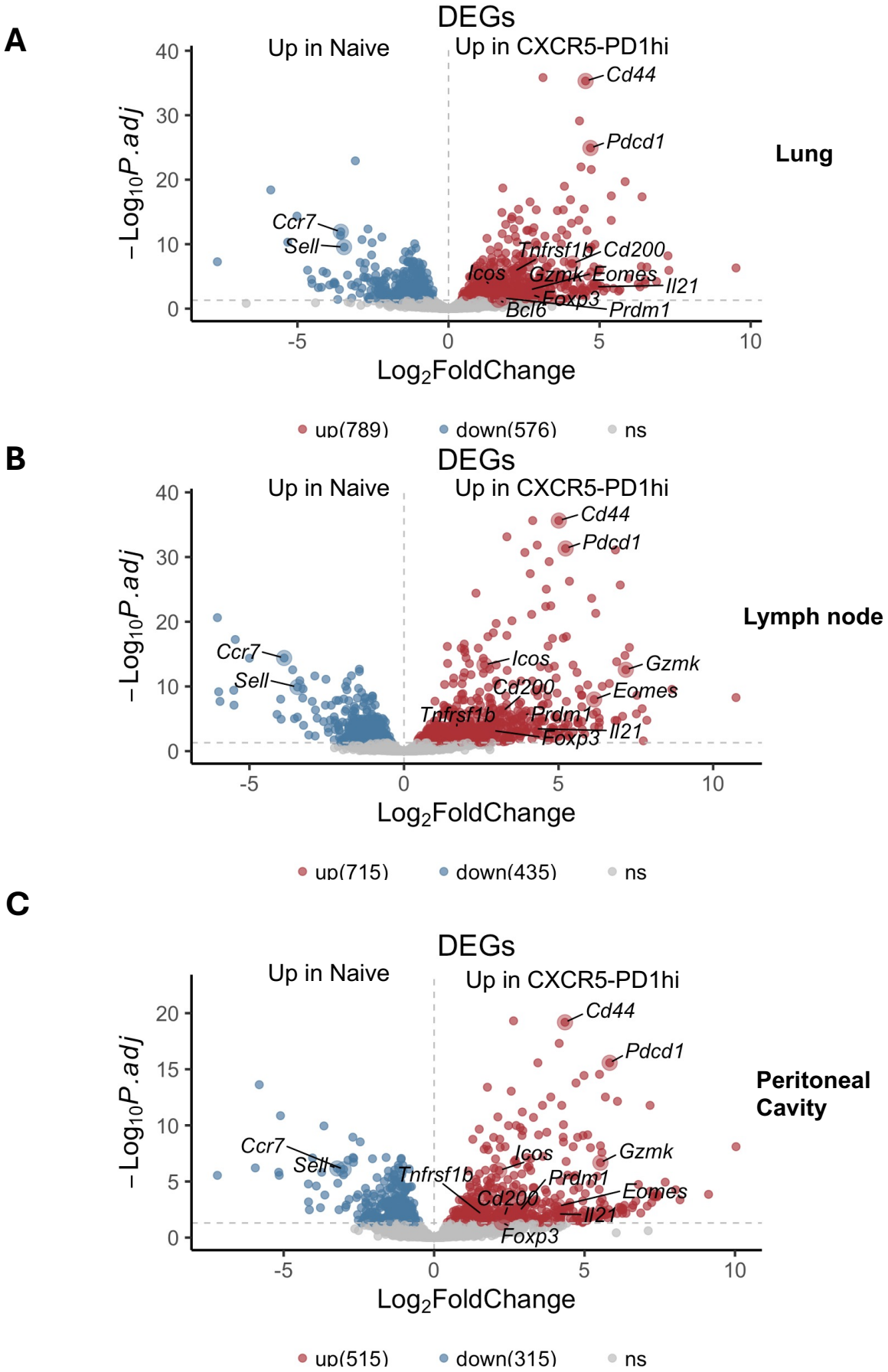

Supplementary Figure 5

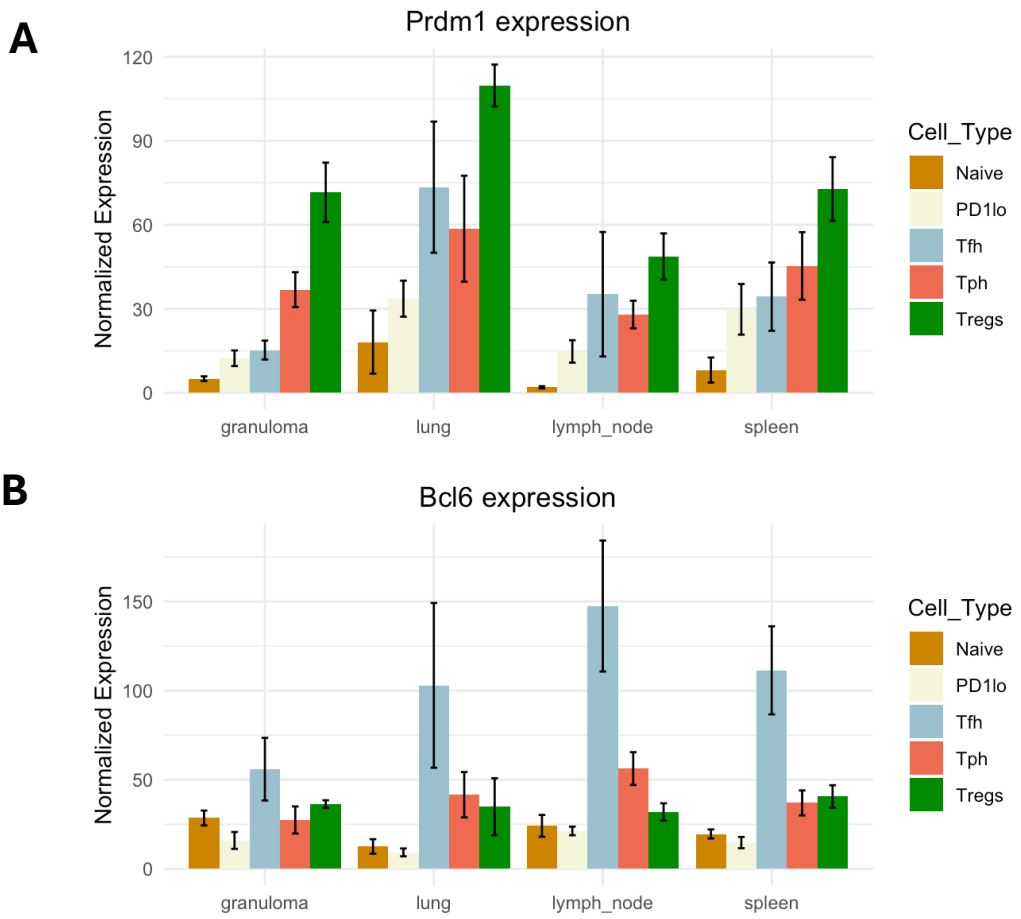

Supplementary Figure 6

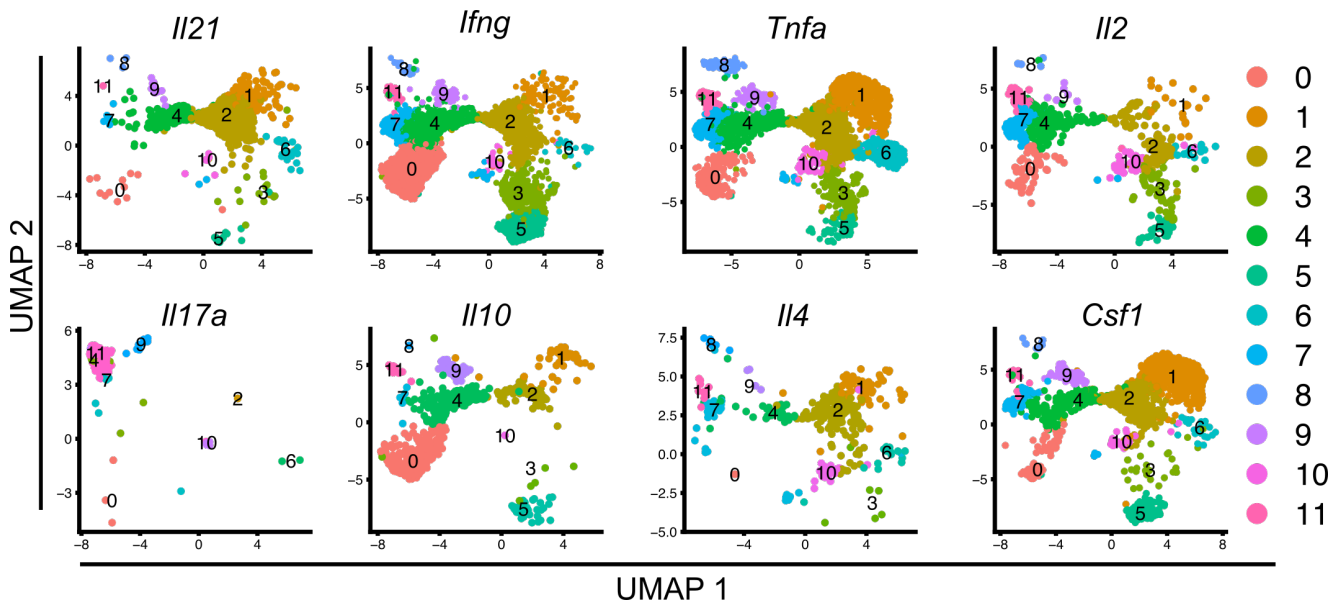

Supplementary Figure 7

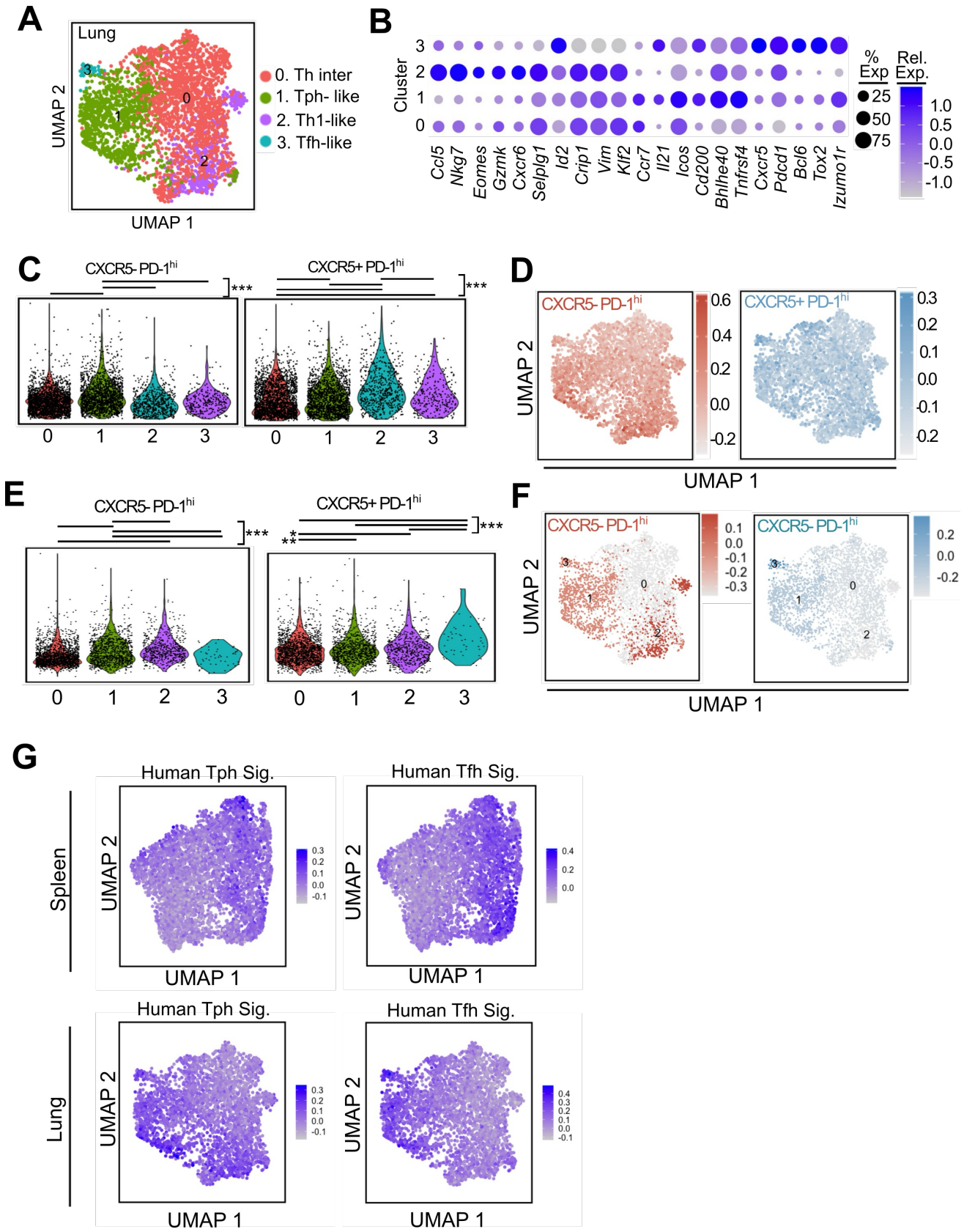
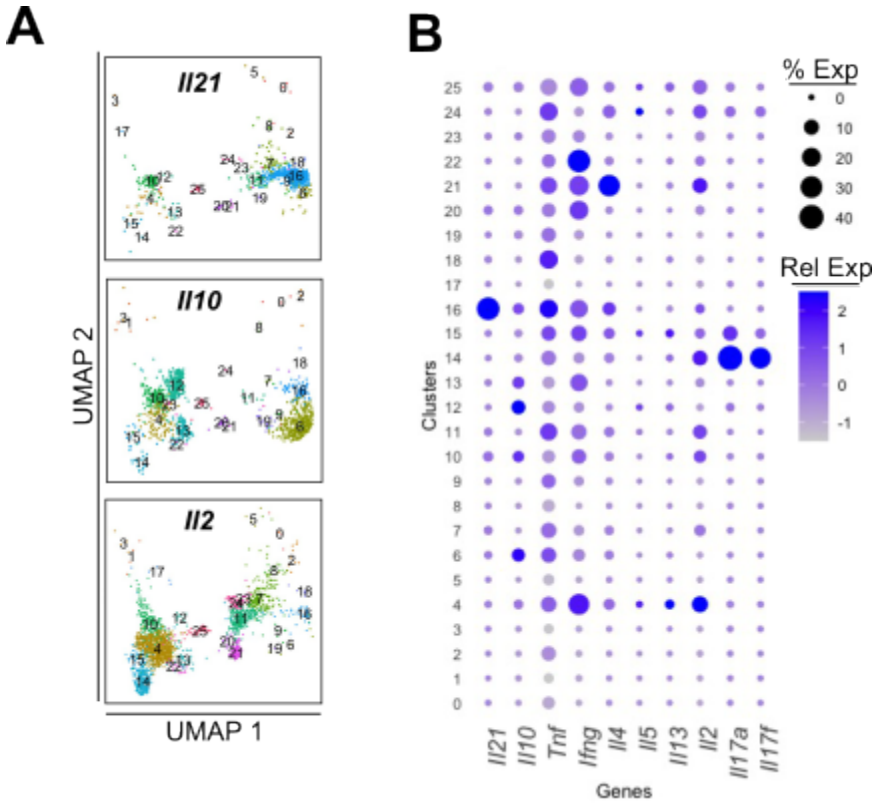
Supplementary Figure 8